

MECHANICAL PROPERTIES OF EPOXY MATRIX COMPOSITE
REINFORCED WITH MULTI-WALLED CARBON NANOTUBES

A THESIS SUBMITTED TO
THE GRADUATE SCHOOL OF NATURAL AND APPLIED SCIENCES
OF
MIDDLE EAST TECHNICAL UNIVERSITY

BY

KEVSER YÜCEER

IN PARTIAL FULFILLMENT OF THE REQUIREMENTS
FOR
THE DEGREE OF MASTER OF SCIENCE
IN
AEROSPACE ENGINEERING

DECEMBER 2019

Approval of the thesis:

**MECHANICAL PROPERTIES OF EPOXY MATRIX COMPOSITE
REINFORCED WITH MULTI-WALLED CARBON NANOTUBES**

submitted by **KEVSER YÜCEER** in partial fulfillment of the requirements for the degree of **Master of Science in Aerospace Engineering Department, Middle East Technical University** by,

Prof. Dr. Halil Kalıpçılar
Dean, Graduate School of **Natural and Applied Sciences**

Prof. Dr. İsmail Hakkı Tuncer
Head of Department, **Aerospace Engineering**

Prof. Dr. Demirkan Çöker
Supervisor, **Aerospace Engineering, METU**

Examining Committee Members:

Assoc. Prof. Dr. Ercan Gürses
Aerospace Engineering, METU

Prof. Dr. Demirkan Çöker
Aerospace Engineering, METU

Prof. Dr. Arcan Dericioğlu
Metallurgical and Materials Engineering, METU

Prof. Dr. H. Emrah Ünalın
Metallurgical and Materials Engineering, METU

Prof. Dr. K. Levend Parnas
Mechanical Engineering, TED University

Date: 27.12.2019

I hereby declare that all information in this document has been obtained and presented in accordance with academic rules and ethical conduct. I also declare that, as required by these rules and conduct, I have fully cited and referenced all material and results that are not original to this work.

Name, Surname: Kevser Yüceer

Signature:

ABSTRACT

MECHANICAL PROPERTIES OF EPOXY MATRIX COMPOSITE REINFORCED WITH MULTI-WALLED CARBON NANOTUBES

Yüceer, Kevser
Master of Science, Aerospace Engineering
Supervisor: Prof. Dr. Demirkan Çöker

December 2019, 69 pages

Improving usage preference of composite material in the aerospace industry brings the requirement of improving mechanical properties of the material. In this thesis, mechanical improvement of epoxy composite materials is analyzed with contribution of functionalized multi-walled CNT with carboxyl group (-COOH) and non-functionalized MWCNT with epoxy for CNT weight fractions of 0.8, 1.0, 1.2, 1.5 and 2.0 wt%. The nanomaterial is dispersed in epoxy resin by calendaring mixing method. Functionalization of CNT provides a good wetting of the reinforcement with epoxy matrix due to additional chemical bonding. The fracture toughness is measured using single-edge notch bending tests, flexural strength using three-point bending tests and tensile strength is measured by carrying out tensile tests. In addition, dynamic mechanical analysis is performed to characterize the material. The fracture toughness and storage modulus of reinforced composites are approximately the same with the base material. Fracture toughness is found not to increase for the weight fractions measured. The composites containing 1.5 wt% MWCNT-COOH and 1.2 wt% MWCNT exhibit increases in tensile strength by 20% and flexural strengths by 15%.

Keywords: Composite, Carbon Nanotubes, Calendering

ÖZ

ÇOK DUVARLI KARBON NANOTÜPLER İLE GÜÇLENDİRİLMİŞ EPOKSİ BAZLI KOMPOZİTLERİN MEKANİK ÖZELLİKLERİ

Yüceer, Kevser
Yüksek Lisans, Havacılık ve Uzay Mühendisliği
Tez Danışmanı: Prof. Dr. Demirkan Çöker

Aralık 2019, 69 sayfa

Havacılık sanayisindeki kullanım alanı artışı, kompozit malzemelerdeki mekanik özellik iyileştirme ihtiyacını getirmektedir. Kompozit malzemelerin fonksiyonlaştırılmamış çok duvarlı karbon nanotüpler (ÇDKNT) ve karboksil (-COOH) moleküler grubu ile fonksiyonlaştırılmış çok duvarlı karbon nanotüpler (ÇDKNT-COOH) ile güçlendirilmiş kompozit malzemelerin mekanik özelliklerindeki iyileşmeler incelenmektedir. Nano-malzemeler kalenderleme yöntemi ile epoksi matris içerisine karıştırılmaktadır. Karbon nanotüplerin -COOH moleküler grubu ile fonksiyonlaştırılması, güçlendirici malzemenin matris ile fazladan kimyasal bağ oluşturamadığı için epoksi ile daha iyi ıslanmasını sağlayamamıştır. Tek kenarda çentik ile bükme yöntemi ile kırılma tokluğu, 3 noktadan bükme yöntemi ile eğilme dayanımı ve çekme dayanımını ölçmek için mekanik testler yapılmıştır. Ek olarak, malzeme karakterizasyonu için dinamik mekanik analiz yapılmıştır. Güçlendirilmiş malzemelerin kırılma tokluk ve saklama modül değerleri baz malzeme ile neredeyse aynıdır. ÇDKNT-COOH ile güçlendirilmiş ve ÇDKNT ile güçlendirilmiş kompozitler baz malzeme ile karşılaştırıldığında çekme dayanımında %20'ye kadar, eğilme dayanımında %15'e kadar iyileşme göstermektedir.

Anahtar Kelimeler: Kompozit, Karbon Nanotüpler, Kalenderleme

I dedicate my thesis to my family.

ACKNOWLEDGEMENTS

Foremost, I would like to express my sincere gratitude to my advisor Assoc. Prof. Dr. Demirkan Çöker for the continuous support of my MS study and research, for his patience, motivation, enthusiasm, and immense knowledge. His guidance helped me in all the time of research and writing of this thesis. I would also like to thank him for his friendship and great sense of humor. I lastly thank him for giving me more time than his toddler for some days.

My sincere thanks also go to my former supervisor Onur Aydemir and my current supervisor Celal Onur Alkaş for leading me working on exciting projects and their acceptance, patience, empathy and support during my research. I would like to special thank them for communicating and finding a way out with me for all the troubles.

The study is performed with the great support of my company, Turkish Aerospace, Inc. I thank all my colleagues in Turkish Aerospace, Inc. uneven work-sharing and for their support during my research. I would like to express a special thanks to my perfect colleague and friend Suna Özkan for her limitless support, settlement for my increasing anxiety as time progressed and keeping me up to date with our projects.

I am extending my thanks to Nanografi for their support during my research work. I also thank the staff of the firm for their kindness.

Also, I thank my friends: Yezdan Medet Korkmaz, Dilan Özdil, Gülce Öztürk, Başak Okumuş, Eren Kozan and Kerem Dönmez for being with me and walking with me all the time.

Last but not the least, I would like to thank my family: my parents Halil İbrahim Yüceer and Şelale Yüceer, for giving birth to me at the first place and supporting me spiritually throughout my life; my one and only sister Ceren Yüceer for giving me her friendship as much as sisterhood and timeless, unconditional support. I also would like to thank my cousins Cemre Terzi and Beyza Erduran for keeping me alive during the study.

TABLE OF CONTENTS

ABSTRACT	v
ÖZ	vii
ACKNOWLEDGEMENTS	x
TABLE OF CONTENTS	xii
LIST OF TABLES	xiv
LIST OF FIGURES	xv
1. INTRODUCTION	1
1.1. Carbon Nanotubes	4
1.2. Functionalized Carbon Nanotubes	8
2. METHODOLOGY	11
2.1. Three Roll Milling	12
2.2. Vacuum Oven and Cure Cycle	17
2.3. Routing and Grinding of Specimens	21
2.4. Discussion	22
3. EXPERIMENTAL PROCEDURE	25
3.1. Fracture Toughness Test	25
3.2. Flexural Tests	27
3.3. Tensile Tests	28
3.4. Dynamic Mechanical Analysis	30
4. RESULTS AND DISCUSSION	33
4.1. SEM Images	33
4.2. Fracture Toughness	38

4.3. Flexural Strength	41
4.4. Tensile Strength.....	43
4.5. Dynamic Mechanical Analysis.....	45
5. CONCLUSION	49
REFERENCES	51
6. APPENDICES.....	55
A. CNT Reinforced Epoxy Polymer Composite Specimen Data per ASTM Standards	55
B. MWCNT/Epoxy Polymer Dispersion by Three-Roll Mill Data	56
C. Manufacturing Data	58
C1. Designed Casting Tool	58
C2. Specimen Routing Data.....	59
D. Raw Test Data	60
D1. SENB Fracture Toughness Test.....	60
D2. Flexural Tests.....	61
D3. Tensile Tests	62
E. Graphed Test Results	63
E1. Load and Displacement Plots for SEN(B) Fracture Tests	63
E2. Stress-Strain Plots for Flexural Tests	65
E3. Stress-Strain Plots for Tensile Tests	67
E4. Plots for Dynamic Mechanical Analysis.....	69

LIST OF TABLES

TABLES

Table 1: Cure Cycle Parameters	11
Table 2: Epoxy Resin Matrix Specifications.....	12
Table 3: CNT Types and Properties	12
Table 4: Mixture data and fracture of MWCNT and epoxy.....	15

LIST OF FIGURES

FIGURES

Figure 1: Distribution of 0.1 vol% macro and nano fillers in aa reference matrix volume of 1 mm ³ a) carbon fiber, particle number of 255 b) carbon nanofiber, particle number of 6.58x10 ⁴ c) carbon nanotube, particle number of 4.42x10 ⁸ [8].....	3
Figure 2: Electron micrographs of microtubules of graphitic carbon a) 5-wall tube with diameter of 6.7 nm; b) 2-walled tube with diameter of 5.5 nm; c) 7-walled tube with diameter of 6.5 nm in largest, 2.2 nm in smallest; d) clinographic view of possible structural model for graphitic tubule [24]	5
Figure 3: a) A graphene sheet made of C atoms placed at the corners of hexagons forming the lattice with arrows AA and ZZ denoting the rolling direction of the sheet to make b) an (5,5) armchair and c) a (0,0) zigzag nanotubes, respectively [19]	6
Figure 4: Three roll mill mechanism	13
Figure 5: Three roll mill structure (dimensions in 619 mm x 356 mm x 381 mm)...	14
Figure 6: Suspension preparation a) Measurement of MWCNT in dust condition, b) MWCNT in pouring container c) MWCNT hand mixed into epoxy in pouring container	15
Figure 7: Three roll mixing process of 1.2 wt% MWCNT-COOH and 400 g epoxy; a) first cycle-beginning at 3 min of endurance at 20 rpm, b) first cycle-finish with 23 min endurance at 20 rpm, c) second cycle with 23 min endurance at 20 rpm, d) fifth cycle with 13 min endurance at 28 rpm	16
Figure 8: Three roll mixing process of 1.5 wt% MWCNT and 400 g epoxy; a) first cycle with 21 min endurance at 20 rpm, b) second cycle with 17 min endurance at 20 rpm, c) third cycle with 8 min endurance at 25 rpm, d) sixth cycle with 7 min endurance at 30 rpm.....	17
Figure 9: Cure oven with vacuum system.....	18

Figure 10: Hand mixing of MWCNT reinforced epoxy and hardener prior to casting a) pouring of hardener, b) hand blender mixing.....	18
Figure 11: Casting of MWCNT reinforced and neat epoxy prior to curing.....	19
Figure 12: Locating of tools into oven prior to curing.....	19
Figure 13: Optimization of oven and vacuum process – inappropriate surface quality	20
Figure 14: Demolded specimens, 1.0 wt% COOH-MWCNT-epoxy, b) 1.2 wt% MWCNT-epoxy, c) 2.0 wt% MWCNT-epoxy.....	20
Figure 15: 3-axis CNC routing of specimen plate.....	21
Figure 16: Machining of specimens for notch structure	21
Figure 17: Photomicrograph of notched specimens a) before crack opening of 0.8 wt% MWCNT-COOH/polymer composite, b) after crack opening of 0.8 wt% MWCNT- COOH/polymer composite.....	25
Figure 18: SENB test fixture with located specimen.....	26
Figure 19: Crack propagation during experimental measuring of fracture toughness	26
Figure 20: Flexural test fixture with a) located specimen, b) specimen under load..	27
Figure 21: Tensile test fixture with mis-located specimen, a) before fracture b) after fracture	29
Figure 22: Tensile test fixture with specimen, a) before fracture b) after fracture....	30
Figure 23: 3-point bending test fixture with located specimen for DMA.....	31
Figure 24: SEM images of 0.8 wt% MWCNT reinforced epoxy matrix composite a) with carboxyl-functionalized MWCNT reinforcement at 50,000x magnification (left), at 100,000x magnification (right); b) with non-functionalized MWCNT reinforcement at 50,000x magnification (left), at 100,000x magnification (right).....	34
Figure 25: SEM images of 1.0 wt% MWCNT reinforced epoxy matrix composite a) with carboxyl-functionalized MWCNT reinforcement at 50,000x magnification (left), at 100,000x magnification (right); b) with non-functionalized MWCNT reinforcement at 50,000x magnification (left), at 100,000x magnification (right).....	35

Figure 26: SEM images of 1.2 wt% MWCNT reinforced epoxy matrix composite a) with carboxyl-functionalized MWCNT reinforcement at 100,000x magnification; b) with non-functionalized MWCNT reinforcement at 100,000x magnification.....	36
Figure 27: SEM images of 1.5 wt% MWCNT reinforced epoxy matrix composite a) with carboxyl-functionalized MWCNT reinforcement at 50,000x magnification (left), at 100,000x magnification (right); b) with non-functionalized MWCNT reinforcement at 50,000x magnification (left), at 100,000x magnification (right).....	37
Figure 28: Load and displacement plot for initial crack length of 1.0 cm with $a/W = 0.4$	39
Figure 29: Fracture toughness of MWCNT reinforced epoxy matrix composite and base epoxy with different fractions.....	40
Figure 30: 1.5 wt% non-functionalized MWCNT reinforced epoxy specimens a) standard fracture surface, b) fracture surface with air bubbles	41
Figure 31: Flexural stress-strain curves of MWCNT reinforced epoxy matrix composite and base epoxy with different fractions	42
Figure 32: Flexural strength of MWCNT reinforced epoxy matrix composite and base epoxy with different fractions	43
Figure 33: Tensile properties of MWCNT reinforced epoxy matrix composite and base epoxy with different fractions	44
Figure 34: Tensile strength of MWCNT reinforced epoxy matrix composite and base epoxy with different fractions	45
Figure 35: Storage modulus of non-functionalized and carboxyl-functionalized MWCNT reinforced epoxy matrix composite and base epoxy with different fractions	46
Figure 36: Tan delta of non-functionalized and carboxyl-functionalized MWCNT reinforced epoxy matrix composite and base epoxy with different fractions	47
Figure 37: Glass transition temperature of non-functionalized and carboxyl-functionalized MWCNT reinforced epoxy matrix composite and base epoxy with different fractions.....	47

CHAPTER 1

INTRODUCTION

Composite materials have been widely used in many industries. In aerospace industry, usage rate of composite materials, such as carbon or glass fiber reinforced thermoset matrix, is around 50-60% for commercial aircraft [1], where this rate is generally valid for skin and cosmetic parts. Preference for monolithic metallic material over composite material in aerospace structures results from that the weak bridging mechanism between fiber as reinforcement and resin as matrix reduces the mechanical properties through the thickness [2]. Because of the reducing mechanical properties, the interfacial failure between plies and its propagation, known as delamination, occurs; it is a major drawback of composite laminates. In order to make the composite materials preferable to aluminum for structural parts, they need to be improved in terms of toughness and strength. Here, nanomaterials are very promising reinforcement materials due to their superior mechanical properties compared to other existing materials [3, 4].

Carbon nanotubes (CNTs), graphitic carbon nanofibers (GCNFs), graphite nanoplatelets and graphene carbon black (1 atom thick layer formed tightly bonded carbon atoms) have been used as reinforcement nanomaterials in recent studies. CNT and CNF utilization can increase the usage percentage of composite materials in an aircraft due to achieved superior mechanical properties compared to other nanomaterials.

Composite parts are improved in case of physical properties and flourishing as a primary load carrying members in complex shapes. However, the weakness of the material at curved region makes use of complex shape problematic. Those curved regions of a structures can be enhanced by use of CNTs or CNFs, which are nano-

scale structured materials made of pure carbon. Arca and Çöker [5] investigated the effect of adding CNTs in a CFRP composite on the mode-I and mode-II fracture toughness in addition to curved beam strength. A three-phase composite material was obtained by mixing 3 wt% CNTs with epoxy matrix mechanically and hand layup it on dry carbon fiber fabrics. Fracture toughness of CNT added composites was found to increase 25% and 10% compared to base laminate in contrast to curved beam strength which decreased by 50% [5]. Safadi, et al. [6] found that strength increases with increasing CNT concentration. The addition of 2.5 wt% MWCNTs was also found to increase tensile modulus of polystyrene solution by approximately 100%. For studies of lower contents of nanomaterials, CNT weight fraction of 1.0% reinforced polymer composites were demonstrated to increase the elastic stiffness by 30-42% and tensile strength by 25% compared to base polymer [7].

CNTs can be structural (modulus, tensile strength, resistance to fracture) or functional (electrical and thermal conductivity) composite reinforcements. Although, the mechanical properties of nanomaterials are excellent, in most studies, the measured mechanical properties are not as high as expected. This is attributed to the non-uniform dispersion of agglomerated CNTs, and insufficient adhesion of CNTs to the polymer matrix. Several dispersion techniques are studied in the literature including shear mixing, calendering, extrusion, ultrasonic and ball milling [8]. The studies have performed to improve dispersion techniques of CNTs to integrate them as an effective reinforcement in composites which can be achieved by good adhesion between the nanomaterial reinforcement and polymer matrix. Here, mixing technique and chemical structure of CNTs are important. Previous CNT/polymer composite studies have problem of dispersion of entangled CNT because the nanomaterial has extremely large surface area. In Figure 1, it is shown computationally that a 0.1 vol% CNT micro-scale filling in 1 mm³ polymer matrix is denser than other filler materials due to larger quantity because of the differences in density, dimension and geometry. CNT particles exhibit large surface area which is an interface for stress transfer but also responsible for the strong tendency of particles to agglomerate [9, 10]. The

agglomeration of CNTs after dispersion into matrix is also an adverse effect. It should be avoided by stabilizing the nanomaterial in the matrix. These are the reasons why dispersion of CNTs in a polymer matrix is more difficult than other fillers.

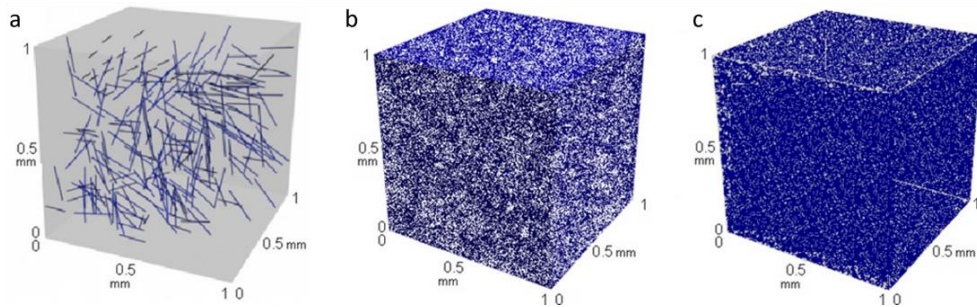


Figure 1: Distribution of 0.1 vol% macro and nano fillers in a reference matrix volume of 1 mm^3 a) carbon fiber, particle number of 255 b) carbon nanofiber, particle number of 6.58×10^4 c) carbon nanotube, particle number of 4.42×10^8 [8]

In the literature, the most productive CNT dispersion method is reported to be calender machine. Calendering known as three roll mills employing shear force created by rollers to mix, disperse or homogenize viscous materials; calender is a standard method to disperse micro-scaled particles in cosmetic, paint and coating industries [11, 12]. The CNT/polymer nanocomposite manufactured by this method is shown as the best in terms of the flexural properties amongst the five techniques used which are ultrasonication applying ultrasound energy to agitate particles in a solution; calendering; ball milling grinding under high pressure created by the collision between tiny, rigid balls in a concealed container; stir dispersing CNT particles in liquid polymers (after several hours of curing reaction, re-agglomerated CNT particles are observed); and extrusion dispersing CNT particles into solid polymers by thin screw rotating at high speed and creating shear flow (this technique is useful for high filling content of CNT) [8]. Dispersion using three roll mills is found to be the most productive method. Dispersion of CNT into epoxy matrix by calender method is more efficient in terms of homogeneity than sonication method. The agglomeration is observed to be smaller than $1.5 \text{ }\mu\text{m}$ with calender method in contrast to sonication method which have agglomeration larger than $2.0 \text{ }\mu\text{m}$. This better performance is attributed to the calender method applying shear force to the whole suspension

structure turning on rolls whereas the sonication method mixes the suspension with local energy application [11].

The improvement effect of CNTs on mechanical properties are observed at lower fractions between 0.1% and 2.0% [13-18]. The agglomeration occurs beyond the reinforcement with weight fraction of 0.5%. Tarfaoui et al. [19] found a degradation in mechanical properties at CNT volume fraction higher than 2.0; that is explained by the viscosity of the dispersion highly increases and the mechanical properties gets lower due to agglomeration and air bubbles appeared at 4.0% volume fraction of CNT into epoxy matrix.

In this study, the effect of increasing MWCNT fraction in epoxy resin is focused. The dispersion technique is settled as calender method via three-roll mill machine. Functionalization of the nanotubes positively contributes to the mechanical properties of composites due to their enhanced dispersion and strong affinity with the epoxy matrix [20]. SEM images of the dispersions proves that the functionalization of CNTs is an effective method for preventing agglomeration of CNTs. The presence of functional groups not only affects the interfacial interactions between polymer matrix and CNTs but also improves the wettability and dispersibility in the liquid matrix; those led to an altered interfacial bonding with the composite [21-23]. Therefore, functionalized MWCNT with carboxyl (-COOH) group is compared with non-functionalized MWCNT for the same weight fractions. The investigation of mechanical properties variation due to CNT volume in epoxy resin and functionalization of CNT is performed in terms of toughness and strength. In order to evaluate the storage modulus and glass transition temperature of the new composite material, dynamic mechanical analysis is performed. The dispersion grade is determined via scanning electron microscope images.

1.1. Carbon Nanotubes

In the mid-1980s, first observed closed convex structure formed by 60 carbon atoms was C₆₀ molecule; the structure named as buckminsterfullerene by the name of

an architect designing geodesic domes, R. Buckminster Fuller. Later, in 1991, the first observation of carbon nanotubes, those are long, slender, tube-structures formed of fullerene, is made by Iijima who is the pioneer of CNT researches [24].

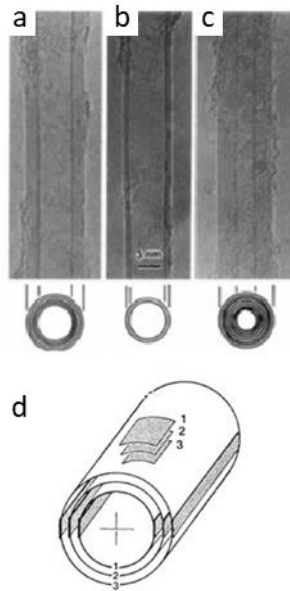


Figure 2: Electron micrographs of microtubules of graphitic carbon a) 5-wall tube with diameter of 6.7 nm; b) 2-walled tube with diameter of 5.5 nm; c) 7-walled tube with diameter of 6.5 nm in largest, 2.2 nm in smallest; d) clinographic view of possible structural model for graphitic tubule [24]

The tube structure of C_{60} molecules is produced by arc-discharge evaporation method, CNTs named as needles and defined as coaxial tubes of graphitic sheets are grown on the negative end of the electrode. The coaxial tubes are 4-30 nanometers in diameter, up to $1\mu\text{m}$ in length. The wall number of the coaxial tubes is ranging from 2 to 50. Those multi-walled tubes' electron graphic and clinographic views are shown in Figure 2, which consist of two or more concentric cylindrical shells of graphene sheets coaxially arranged around a central hollow core with van der Waals forces between the adjacent layers [2].

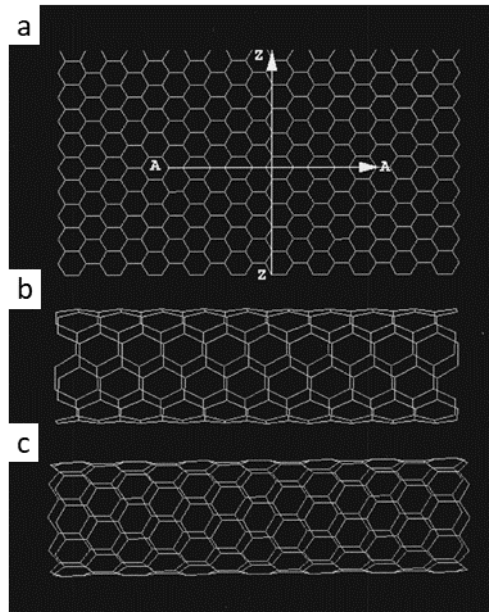


Figure 3: a) A graphene sheet made of C atoms placed at the corners of hexagons forming the lattice with arrows AA and ZZ denoting the rolling direction of the sheet to make b) an (5,5) armchair and c) a (0,0) zigzag nanotubes, respectively [19]

The nature of hexagonal ring structure of the graphene sheet made of carbon atoms leans on giving a positive curvature (convex) to the surface, which leads to close of tube at two ends as shown in Figure 3; the closing structure changes as being armchair or zigzag. Armchair structure seen in Figure 3b is because of the atomic shape perpendicular to the tube axis, and have a symmetry along the axis with a short unit cell with length of 0.25 nm that can be repeated to make the entire section of a long nanotube. The other structure is known as zigzag seen in Figure 3c because of the perpendicular atomic shape to the tube axis, and also have short unit cell with length of 0.43 nm along the axis. All the remaining nanotubes are known as chiral or helical nanotubes and have longer unit cell sizes along the tube axis [19].

Nanocomposites can be agreed as homogeneous materials because of this nano-scale structure. The macro-scale mechanical properties of composite material containing randomly distributed nanomaterials are effectually isotropic when CNTs are well-dispersed. That is, critical point of their excellent mechanical properties. In comparison with traditional fibrous reinforcement, because of the isotropic behavior, CNTs contribution into interphase region is very important for transverse mechanical

properties. That is increasing with increasing CNT volume fraction and decreasing CNT diameter. The CNT effect on mechanical properties in longitudinal direction is negligible [26].

In case of strength, stiffness and other mechanical properties, CNTs are mentioned in place of carbon fiber ultimately. The composites are significantly influenced by interfacial interactions between reinforcement and polymer matrices [4]. Hence, the nanomaterial corresponds to the stiffest material due to micromechanical interlocking, strong chemical bonding and van der Waals force between matrix and reinforcement [9]. CNTs are stronger than diamond since those are composed of sp^2 carbon-carbon bonds and that chemical bonding structure is stronger than sp^3 bonds found in diamond. That case also provides CNTs highest mechanical properties of that any existing material has [27, 28]. The strength of material is 10-100 times of steel at a remarkable weight fraction used in a matrix. Thermal conductivity about twice as high as diamond, electric-current-carrying capacity 1000 times higher than copper wires [3]. However, to proceed the improvement of thermo-mechanical properties of composite materials, it should be noticed, as well as elastic and fracture properties of CNTs, that the interaction at CNT/matrix interface is also a parameter same as fiber composites. The interaction in the interface is supplied by good adhesion of reinforcement with matrix. The qualified load transfer from matrix to the reinforcement composes a set that affects crack propagation or arrest; it strongly depends on the aspect ratio of nanofiber/nanotubes. However, high aspect ratio of nanotubes causes incoming agglomeration due to tending to curling up; as a result of that the strength decreases due to low bending stiffness. That is, agglomeration has material impact on the strength and stiffness of nanocomposites [29].

CNTs are classified in case of their wall types; single-walled, double-walled and multi-walled. Multi-walled carbon nanotubes are the coaxial composing of single-walled nanotubes linking by weak van der Waals forces. The elastic properties of multi-walled structure are independent of the number and radius of layers, the modulus

is the same for all nanotubes with radius larger than 1 nm; likewise, tensile strength and stiffness change are negligible through whole nano-scaled structure [10]. As result of intratubular weak van der Waals forces between the layers of MWCNTs and the transfer loads to the nanotube via shear stress at the reinforcement-matrix interface, the effective stiffness of MWCNT in polymer matrix is reduced. Therefore, SWCNT or DWCNT are more effective for increasing elastic stiffness; however, MWCNT offers significant potential as a possible multifunctional reinforcement due to availability. In other case, high aspect ratio and large interfacial area of MWCNT make it an ideal candidate enhancing electrical and thermal conductivity, toughness, impact resistance and vibration damping [12]. Therefore, in the study, in case of price as a parameter, multi-walled nanotubes are chosen as the reinforcement.

1.2. Functionalized Carbon Nanotubes

The improvement of the interfacial adhesion between polymer matrix and CNTs can be achieved by a chemical functionalization of the nanotube surface. Catalytically grown carbon nanotubes by oxidative treatment includes molecular groups containing oxygen. The functional group, observed as phenolic, carboxylic and lactonic in majority, stabilize dispersion of carbon nanotube in polymer matrix with additional covalent bonding [30].

In the SEM images of functionalized CNT reinforced polymer composite from literature, it is observed that while crack opened nanotubes are failed. This can be a further evidence of the strong interface between nanotube and epoxy matrix. 1.0 wt% addition of functionalized CNT to polymer provides covalent bonding/chemical cross-linking improving interfacial shear strength; therefore, shear strength of the reinforced matrix is enhanced without reducing Young's modulus significantly [31]. The sample containing 1.0 wt% DWCNT-NH₃ showed higher fracture toughness than all other samples with lower fraction and non-functionalized CNTs. That is, constructed polar bonding of functionalized CNTs with polymer matrix improves the toughness of dispersion by crack-bridging mechanism besides the strength. Functionalization of

CNTs has influence on tensile strength, Young's modulus and fracture toughness compared to non-functionalized CNTs with the weight fraction of 0.1 and 1.0. This behavior explained by improving dispersion quality due to strong interaction of functional molecular group with epoxy matrix [11].

CHAPTER 2

METHODOLOGY

In this study, the matrix material is Epikote™ resin MGS® LR 285 and the hardener is Epicure™ curing agent MGS® LH 287 with mixing ratio of 100:40±2 by weight to cure the matrix. Cure cycle parameters are given in Table 1 and material specification per material datasheet are given in Table 2.

Table 1: Cure Cycle Parameters

	Heating Rate [°C/min]	Temperature [°C]	Time [min]	Cooling Rate [°C/min]
Hardening	0.5	45	240	1.0
Post Cure	0.5	85	900	1.0

The reinforcement nanomaterial is CNT; multi-walled CNTs are purchased from Nanografi, the institute researching and developing nanomaterials and nanotechnology. The nanomaterials are manufactured by chemical vapor deposition (CVD) method; physical material properties are given in Table 3. MWCNTs are used in two different chemical structures: functionalized MWCNTs with carboxyl group (-COOH) and non-functionalized MWCNTs. The mechanical behavior is then compared with that of bare epoxy matrix. In addition to the two chemical structures, nanomaterial weight fraction is also varied: 0.8, 1.0, 1.2, 1.5 and 2.0 wt%. Each specimen is cut out of a plate with dimensions adjusted per required test: mode-I fracture toughness, tensile and flexure tests. In addition, the viscoelastic properties are determined by dynamic mechanical analysis (DMA).

Table 2: Epoxy Resin Matrix Specifications

	Laminating Resin LR 285	Hardener LH 287
Density [g/cm³]	1.18 – 1.23	0.93 – 0.96
Viscosity [mPas]	600 - 900	80 - 120
Epoxy equivalent [g/equivalent]	155 - 170	-
Epoxy value [equivalent/100g]	0.59 – 0.65	-
Amine value [mg KOH/g]	-	450 - 500
Refractory index	1.5250 – 1.5300	1.4950 – 1.4990

The mechanical properties of MWCNT reinforced epoxy are characterized with KIC, mode-I fracture toughness by single-edge-notch bending (SENB) method per ASTM D5045-14; flexural strength by 3-point bending method per ASTM D790-03; tensile strength per ASTM D638-14. The specimen numbers 3, 5 and 5 relatively; in the study, the numbers are doubled in case of set up, calibration and failure process. The formulations are given in experimental procedure.

Table 3: CNT Types and Properties

CNT Type	Diameter [nm]	Length [um]	Density [g/cm³]	Purity [%]
MWCNT-COOH	8--18	10--35	0.2	96.0
MWCNT	8--18	10--30	2.6	96.0

2.1. Three Roll Milling

The production of specimens begins with shear mixing of CNT and epoxy resin by using three roll mills of Torrey Hills Technologies. The machine, generally used in cosmetic, pharmacy, ink industries for particles such as pigment integration to

polymer, has three horizontal rollers, each of those rotates in an opposite direction and at two different speeds. The dimension of rollers is 65 mm in diameter and 127 mm in length, and can rotate at speeds up to 432 rpm. The identification and rotating direction of three stainless steel rollers are given in Figure 4. Feeder roll and apron roll rotate in the same direction while center/mid roll in the opposite direction; the rolls rotate faster from feeder roll to apron roll. The center roll is fixed while feeder and apron rolls can be moved to arrange the distance between rolls at micron scale by the screw adjuster.

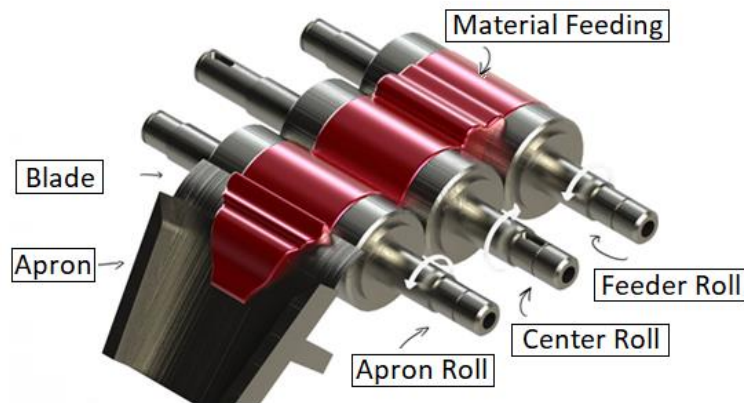


Figure 4: Three roll mill mechanism

Three roll mill works better for the blending of viscous material containing binders such as oil and epoxy according to the many experiments Torrey Hills done. The adjustment of roller distance is critical for not dripping; for the study, the distance between center roll and feeder roll, described as slow rollers in Figure 5, is 20 μm for Epikote™ resin MGS® LR 285; the distance between center roll and apron roll, described as fast roller in Figure 5, is 30 μm . At first cycle of mixing, since the agglomeration is higher, the viscosity of the suspension is higher and residence time is higher. For later cycles, agglomeration reducing, viscosity decreasing and residence time of the suspension is lower. Therefore, being an alternative to fix the gap distance, the time can be standardized by arranging gap between rolls as in study of Thostenson et al. [12].

The suspension is casted by hand on between feeder roll and center roll and moves through other rolls due to tremendous shear force created by rotation in opposite directions described in Figure 5. By that suspensions made of viscous materials can be finely dispersed, mixed, refined or homogenized. The mechanism does not perform a size reduction for those materials; by the shear force, fine particles, which are tend to agglomerate, break apart. As a result, the final fineness depends on the original particle size for the dry ingredients.

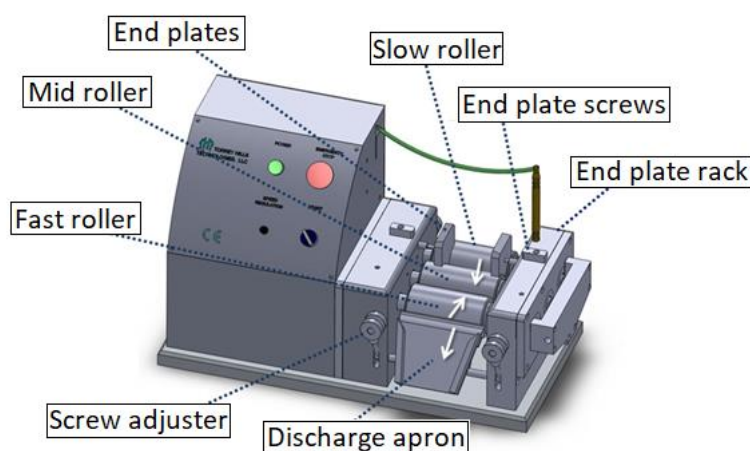


Figure 5: Three roll mill structure (dimensions in 619 mm x 356 mm x 381 mm)

The suspension is gathered and prevented from leaking sideways by the end plates. Discharge apron is located on the apron roll to scrape suspension from the fast roller and carry it to the container. The cycle number is settled as 7 for the study, that is the required number for a visually homogeneous suspension, the speed of each cycle is arranged as 20, 20, 25, 25, 28, 30 and 35 rpm respectively. The speed can be set only for the slower feeder and center roll; the speed of the faster apron roll changes depending on other rolls. Total MWCNT and epoxy quantity is summarized in Table 4 per arranged weight fractions. For each CNT fraction, the suspension is split in two parts for ease of feeding material and period reduction. That is, for each cycle 400 gr of epoxy and MWCNT are measured accordingly as in Figure 6a, and hand mixed as in Figure 6c prior to the feeding of rollers.

Table 4: Mixture data and fracture of MWCNT and epoxy

Reinforced Epoxy Mixture Data			
CNT Type	CNT weight%	Total resin qty [g]	Total CNT qty [g]
MWCNT	0.8%	800	6.4
	1.0%	800	8
	1.2%	800	9.6
	1.5%	800	12
	2.0%	800	16
MWCNT-COOH	0.8%	800	6.4
	1.0%	800	8
	1.2%	800	9.6
	1.5%	800	12
	2.0%	800	16

Dispersion of suspension by shear mixing method results with agglomeration at the end of the first cycle shown in Figure 7a and 7b, hand mixed nanoparticles are adhered each other by applied high shear force with rollers in opposite direction. In the second cycle shown in Figure 7c, agglomerated nanoparticles adhered on the rollers are observed. In the third cycle, nanoparticles start to get wet with epoxy matrix by application of continuous shear force and nanoparticle quantity on the rollers are reducing. In fifth shown in Figure 7d, sixth and seventh cycles, the observed homogeneity of suspension is increasing.



Figure 6: Suspension preparation a) Measurement of MWCNT in dust condition, b) MWCNT in pouring container c) MWCNT hand mixed into epoxy in pouring container

Functionalization of MWCNT improves the dispersion process; since viscosity of suspension is low for each cycle, calender technique is a productive method for MWCNT dispersion into polymer epoxy. However, bridging mechanism of non-

functionalized MWCNT and matrix is without non-covalent linking. Thus, agglomeration of nanoparticles is higher for this case per observation seen in Figure 8a and 8b; in first and second cycles at 20 rpm, the rolls are covered with MWCNT those cannot dispersed in resin. The dispersion homogeneity increases in sixth cycle at 30 rpm as shown in Figure 8d. Increasing pure MWCNT content increases viscosity of suspension and makes it a more difficult dispersion process. Especially for 1.5 and 2.0 weight fraction of non-functionalized MWCNT, the application is inadequate in terms of homogeneous mixing, flatwise casting on tool and uniform laying on fiber reinforcement.

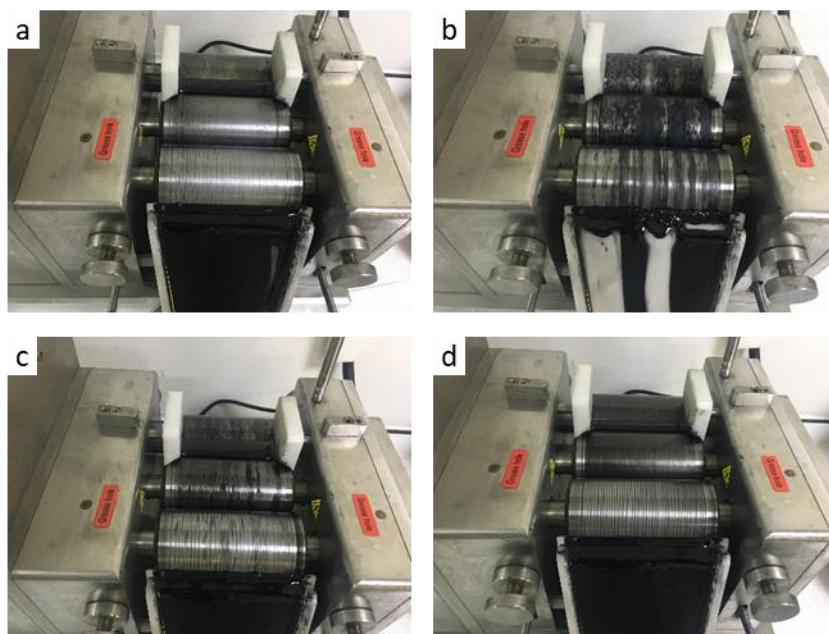


Figure 7: Three roll mixing process of 1.2 wt% MWCNT-COOH and 400 g epoxy; a) first cycle-beginning at 3 min of endurance at 20 rpm, b) first cycle-finish with 23 min endurance at 20 rpm, c) second cycle with 23 min endurance at 20 rpm, d) fifth cycle with 13 min endurance at 28 rpm

The cycle period of non-functionalized MWCNT is 50% shorter in three roll mills as stated in Figure 7 and Figure 8, and appendix B in detail. It is commented as smaller particle size of pure MWCNT compared to MWCNT-COOH decreases the fineness of suspension, and finer suspension move through the rolls faster than MWCNT-COOH. This situation is the proof and the reason of agglomeration. The

agglomeration can be reduced by arranging roll distance as 15 μm and lower in despite of increasing time period of roll cycle.

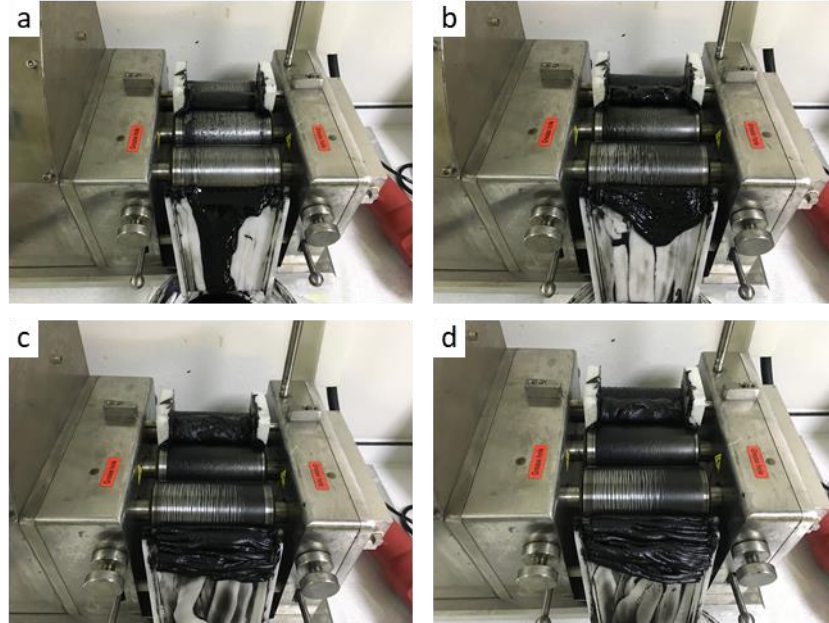


Figure 8: Three roll mixing process of 1.5 wt% MWCNT and 400 g epoxy; a) first cycle with 21 min endurance at 20 rpm, b) second cycle with 17 min endurance at 20 rpm, c) third cycle with 8 min endurance at 25 rpm, d) sixth cycle with 7 min endurance at 30 rpm

2.2. Vacuum Oven and Cure Cycle

Cure cycle of the dispersed suspension is carried out with Vacutherm in Figure 9 from Heraeus Instruments supplied by Turkish Aerospace. Oven is calibrated according to the required cure cycle data given above in Table 1 to harden the epoxy resin. In Figure 10a and 10b, the hardener is poured into the epoxy with a weight ratio of 40:100. The mixing is performed with the hand blender for at least 4 minutes for uniform epoxy-hardener suspension. Hardener dispersion into neat epoxy is applied with only hand mixing for 5 minutes until homogeneous and visually uniform suspension is obtained. After this, the casting should be performed in 75 min before the gel time begins.



Figure 9: Cure oven with vacuum system

The casting tools are designed according to specimen dimensions and oven inner capacity, and manufactured with a 3-axis CNC bench at Turkish Aerospace. Manufacturing data of tools are given in detail in Appendix C. Prior to suspension casting, all tool surface is covered with release agent to prevent adherence of MWCNT-epoxy plate and ease of demolding. The application should be performed twice and the release agent on the tool should be dried before a second application. This process is repeated before every cure cycle.

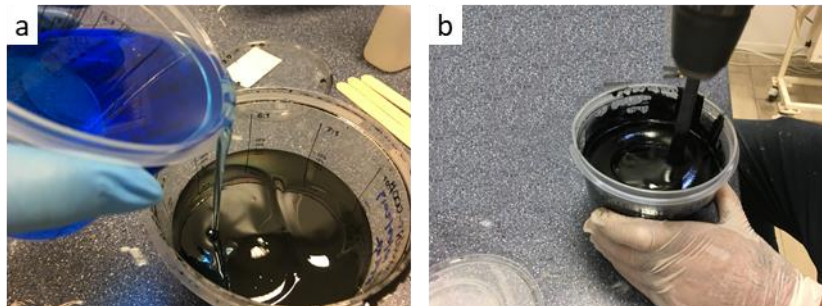


Figure 10: Hand mixing of MWCNT reinforced epoxy and hardener prior to casting a) pouring of hardener, b) hand blender mixing

Following desiccation of release agent and matte visualization obtained on tool surface, casting of suspension is performed as in Figure 11a. Tool depth is arranged as 5 mm deeper than specimen thickness in case of overflowing of dispersion during oven process. The quantity of fluid dispersion to obtain related thickness figured out by the red markings on side tool surfaces.

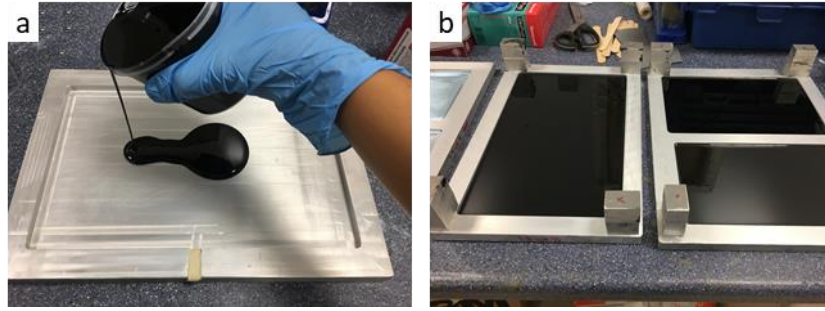


Figure 11: Casting of MWCNT reinforced and neat epoxy prior to curing

Locating tools with spacer as shown in Figure 11b to place four tools at the same time in the oven reduces the cure cycle period of the study. In this way, two suspension with different fractions of MWCNT are cured at one cycle since the cycle parameters change with epoxy type only. However, it is taken into account and taken precaution from that different type of mixtures should not be poured into each other. Two flat positioning is made by four spacers locating inter tools. The tools with suspension poured are placed in the oven as in Figure 12a and 12b.

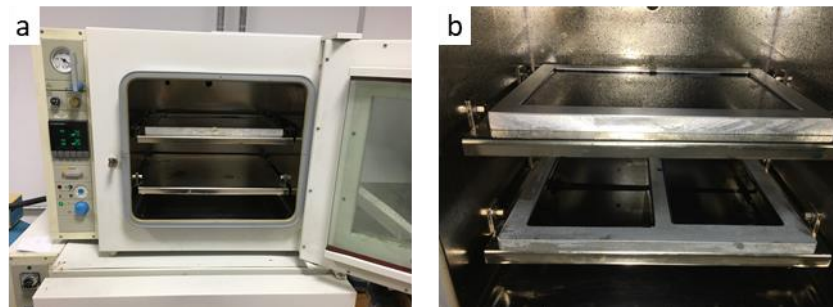


Figure 12: Locating of tools into oven prior to curing

In the study, vacuum oven is preferred because air inside of fluid suspension should be exhausted. Otherwise, cavity structure of epoxy plate decreases the stiffness and strength of the material. Vacuum application process is not standard in literature; therefore, primarily, the optimization of vacuum process is performed. If full vacuum is applied during the whole period of the cure cycle, during the completion of the gel time period (75-120 minutes), craters on the surface are created during the air leaving the suspension and other air bubbles remain in the suspension. The surface quality during air exit is shown in Figure 13a and 13b.

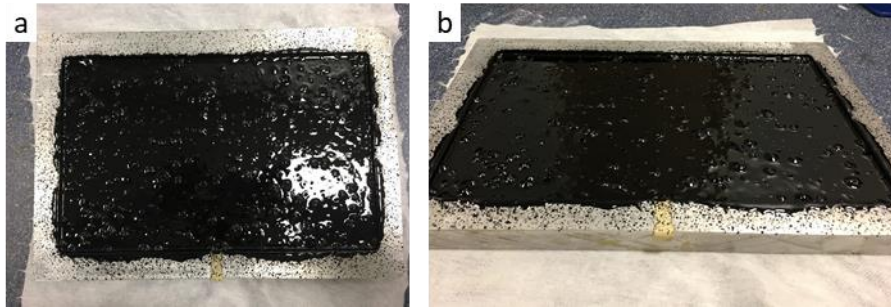


Figure 13: Optimization of oven and vacuum process – inappropriate surface quality

In our case, the material gel time is 80 minutes so that the vacuum process has to be completed before the gel time. Application of vacuum occurs before gel time starts at 80 minute of curing process. However, especially for non-functionalized MWCNT reinforced epoxy mixture with higher density, the surface quality is inadequate due to air inside the cured plate. Adequacy of surface quality is provided by application of vacuum at room temperature, 25-35°C, without starting cure cycle for 80 minutes duration. After this period is completed, the vacuum is switched off, air outlet completed and oven inside pressure is set to the atmospheric pressure, 1 atm. During the air outlet, air bubbles disappear from the surface. Subsequently, the oven is turned on and cycle is started up according to the calibrated cure program.



Figure 14: Demolded specimens, a) 1.0 wt% COOH-MWCNT-epoxy, b) 1.2 wt% MWCNT-epoxy, c) 2.0 wt% MWCNT-epoxy

Improved surface quality can be observed in Figure 14a for functionalized MWCNT with -COOH group. However, for the surface of non-functionalized MWCNT reinforced epoxy, shown in Figure 14b, the quality declines with increasing weight fraction of CNTs. The reason is difficulty of air outlet with increasing viscosity of suspension and increasing agglomeration. The surface roughness for 2.0 wt% of pure MWCNT, shown in Figure 14c, is unacceptable even for routing process.

2.3. Routing and Grinding of Specimens

Specimens are machined at 3-axis CNC machine at Turkish Aerospace Company shown in Figure 15. Plate dimensions are settled according to the specimen dimensions and numbers per ASTM standards of required tests to characterize the new CNT reinforced epoxy composite material. For each test, a plate is designed and dimensioned, designed plate parameters are given in Appendix A and specimen dimensions cut out from plate are given in Appendix C2 in detail.

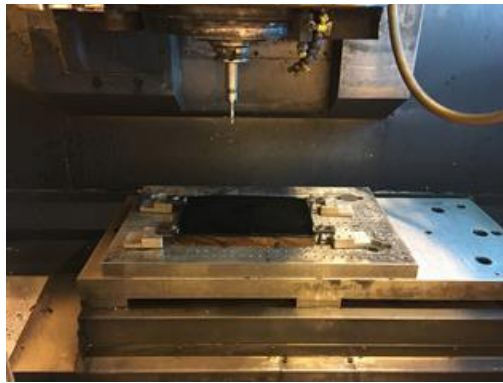


Figure 15: 3-axis CNC routing of specimen plate

To fix the plate for routing process, standard fixture plates with holes are utilized, specimen located on wood stand and fixed on fixture by standard fasteners with bracket supports as shown in Figure 15. In case of material brittleness, hardness and elasticity, in addition to fixing points, speed of spindle, size of cutter and amount of cooling liquid are also parameter. Those are optimized during first routing processes by sacrificing few numbers of specimen.

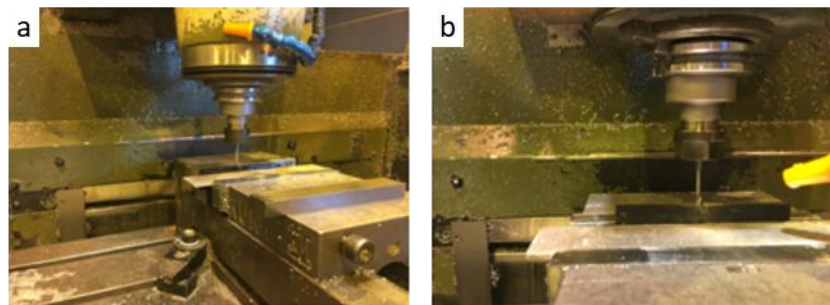


Figure 16: Machining of specimens for notch structure

Following routing operation, the specimen needed to be grinded to provide close tolerance dimensions specified in Appendix C2. Specimens are notched per ASTM standard prior to locating test fixture, the process, that is shown in Figure 16a and 16b, is completed on the 3-axis machine shop controlled by hand. The cutter for the notching is specially machined according to the required notch dimensions and sharpness at the tip. At the end, the specimens are deburred and holding lugs are cut out, they are marked according to the fraction and CNT type and bagged separately for the test.

2.4. Discussion

During the dispersion process, the main differences between the functionalized and non-functionalized CNT specimen types is the viscosity of the suspension. Non-functionalized CNTs are higher in means of volume than carboxyl-functionalized CNTs when the same weight is measured in precision scale to pour into the epoxy. Therefore, for the same calendaring conditions, the agglomeration is observed to be higher and suspension viscosity is higher for the non-functionalized MWCNT/epoxy polymer suspension. Our results indicate that non-functionalized MWCNT may not be producible for higher fractions as discussed in the previous section.

The enhancement in mechanical properties is attributed to specific interactions between the functionalization groups of the CNTs and the polymer matrix [16]. The change in suspension viscosity can be explained as the dispersion quality accomplished in terms of conformity of functionalization group of the reinforcement with the epoxy matrix. That is, non-functionalized MWCNTs are well-dispersed in epoxy since increasing viscosity with increasing weight fraction. However, at high fractions the practical application of MWCNTs into epoxy matrix gets harder since the viscosity of the suspension is too high. Therefore, the MWCNT reinforced epoxy matrix dispersion should be prepared at lower fractions. Furthermore, carboxyl functionalization group of MWCNTs is not compatible with polymer epoxy in terms

of molecular attraction; hence, the viscosity of the functionalized-MWCNT reinforced epoxy matrix dispersions are lower.

Surface quality of cured specimens are better for carboxyl-functionalized MWCNT reinforced epoxy polymer composites. A wavy surface is observed according to the surface radiance of the specimen, which is bright for MWCNT-COOH reinforcement and granular with craters for non-functionalized MWCNT reinforcement. The reason for that is better dispersion of MWCNT-COOH with the epoxy matrix.

CHAPTER 3

EXPERIMENTAL PROCEDURE

3.1. Fracture Toughness Test

Single-edge-notch three-point bending (SENB) test method is performed to measure mode-I fracture toughness per ASTM 5045-14. The specimen has a length of 120 mm, width of 25 mm and thickness of 6.5 mm. Three tests are conducted for each specimen type.

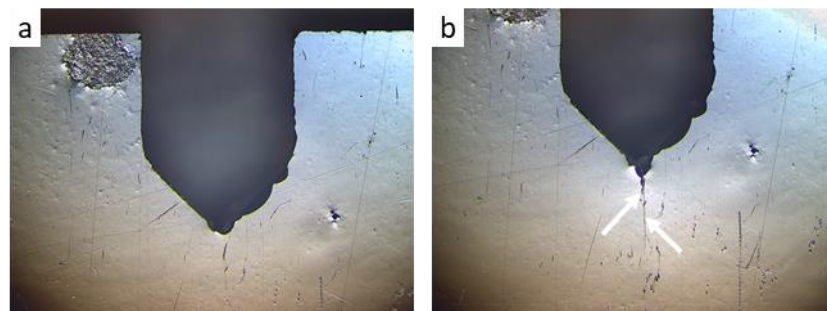


Figure 17: Photomicrograph of notched specimens a) before crack opening of 0.8 wt% MWCNT-COOH/polymer composite, b) after crack opening of 0.8 wt% MWCNT-COOH/polymer composite

To create an initial crack, following notch machining process, specimens are tapped by hand using a sharp nozzle and a plastic hammer. Photomicrographs of the crack tips before and after the tapping are shown in Figure 17a and 17b, respectively. The initial crack length is measured via microscope images at three points on the initial crack front after the fracture test is completed and the specimen is broken into two parts.

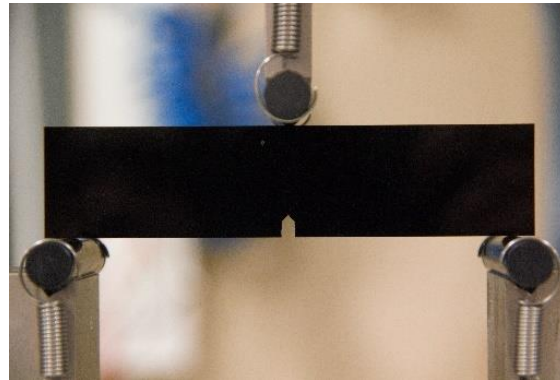


Figure 18: SENB test fixture with located specimen

Prepared specimens are placed in a 3-point bending test fixture with the notch in the bottom as shown in Figure 18. The span of the fixture is 100 mm for a span-to-width ratio of 4:1. The test is conducted under displacement-controlled loading with a crosshead displacement rate of 1 mm/min.

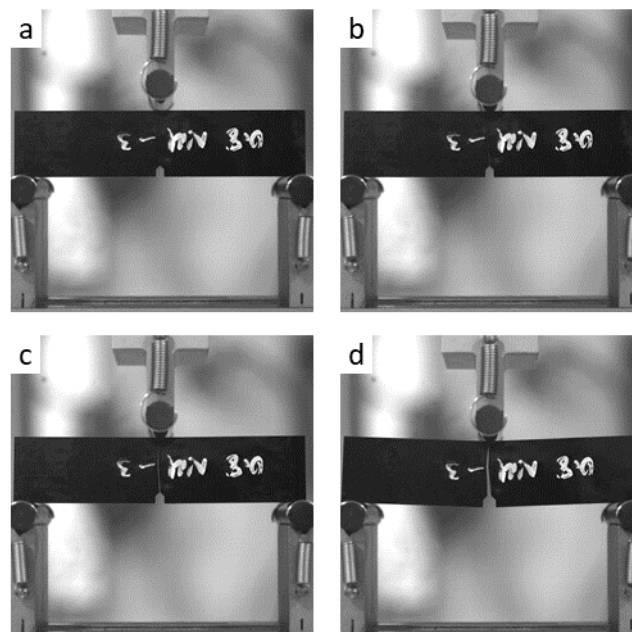


Figure 19: Crack propagation during experimental measuring of fracture toughness

Following the loading of specimen, the crack propagates from the crack tip through the width of specimen, as shown in Figure 19a-19d; The stroke and load are recorded until the crack reaches the end of the specimen width and the recorded maximum load is used to calculate the fracture toughness $K_{IC} = K_Q$ value from,

$$K_Q = \left(\frac{P_Q}{BW^{\frac{3}{2}}} \right) f(x), \quad (1)$$

$$f(x) = 6x^{\frac{1}{2}} \left(\frac{[1.99 - x(1-x)(2.15 - 3.93x + 2.7x^2)]}{(1+2x)(1-x)^{\frac{3}{2}}} \right),$$

$$x = \frac{a_{initial}}{W} \quad \text{where } 0 < x < 1,$$

where, P_Q is the maximum load in kN from the load displacement plot, B is the specimen thickness in cm, W is the specimen width in cm, and a is the initial crack in cm which is average of crack length measured at three points on the initial crack front.

3.2. Flexural Tests

Flexural strength and strain are measured using 3-point bend test per ASTM D790-15 testing standard. For each material, three specimens are cut from the same plate and machined on 3-axis CNC machine per specified dimensions in the test standard: length of 125 mm, width of 12.5 mm and thickness of 3 mm. Three specimens are tested for each case. The specimen placing on test fixture is shown in Figure 20a; the specimen under load is curved just before fracture as shown in Figure 20b.

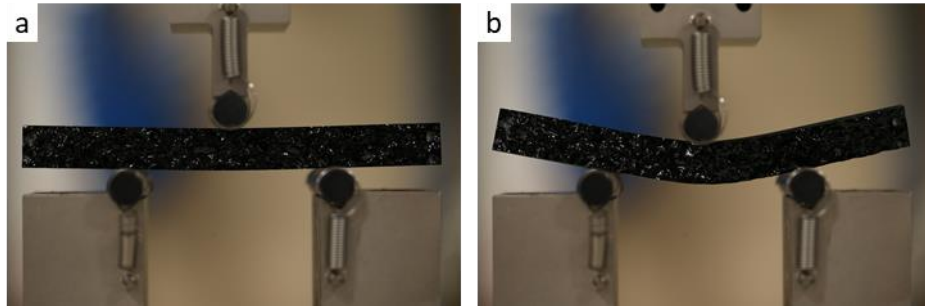


Figure 20: Flexural test fixture with a) located specimen, b) specimen under load

The support span length is set as 60 mm with a span-to-depth ratio of 16:1; here, the depth is average of depth of each specimen to be tested. The displacement rate of crosshead is 2 mm/min according to the test standard. The test should be terminated when the maximum strain occurs, given as 0.05 in the standard. The deflection, D value of the maximum strain is calculated from,

$$D = rL^2/6d, \quad (2)$$

D is calculated as 10 mm from Eq. 2 where r is strain of 0.05, L is support span of 60 mm, and d is specimen depth of 3 mm.

The stroke and load are recorded until the fracture occurs and the recorded maximum load is used to calculate the flexural strength, σ_f and flexural strain, ε_f values from,

$$\sigma_f = 3PL/2bd^2, \quad (3)$$

$$\varepsilon_f = 6Dd/L^2, \quad (4)$$

where, P is the maximum load in kN from the load displacement plot, b is the specimen width in mm, and d is the specimen thickness in mm.

3.3. Tensile Tests

Tensile strength and strain of epoxy matrix composite specimens reinforced with different weight fractions of carboxyl-functionalized MWCNT and nonfunctionalized MWCNT are compared per experimental data with base material. The experiments are performed per ASTM D638-14; the specimens are manufactured as type I specimen with length of 165 mm, width of 19 mm and thickness of 5 mm.

The distance between grips for tensile test is 115 mm per standard, there is requirement for grip length of 25 mm for clamp region at both end through length of the specimen. The speed of test as crosshead displacement rate is 5mm/min. The specimen is located on tensile test fixture as providing grip length of 25 mm and centering on clamp region in width. Stroke of test fixture is set to zero where load is zero and test begins.

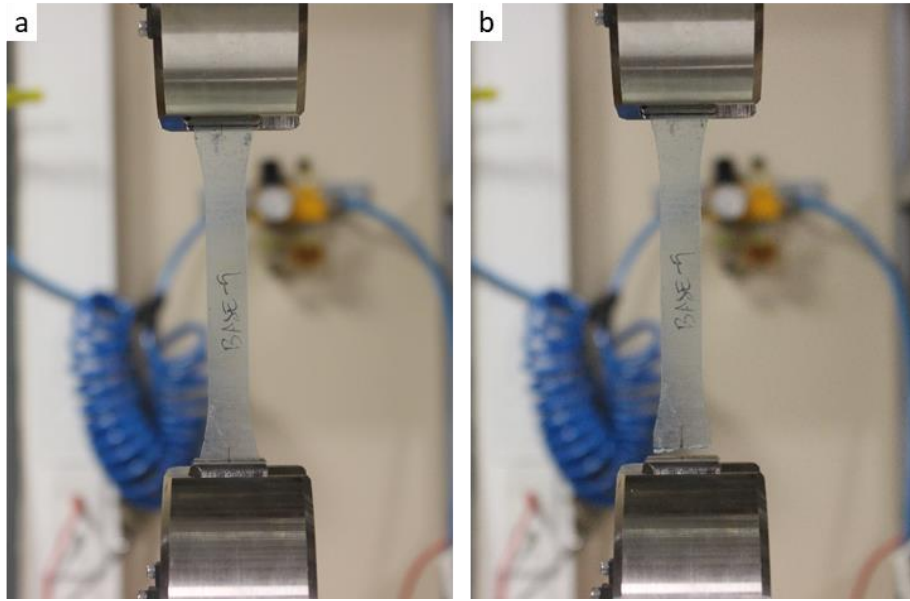


Figure 21: Tensile test fixture with mis-located specimen, a) before fracture b) after fracture

The first three specimens located as in Figure 21a are fractured at unexpected cross sectional area as seen in Figure 21b; to record a correct data during tensile test, the fracture should be occurred through span length of 165 mm. Apart from mis-breaking, the slippage of specimen during test is observed by a load drop and the test is terminated due to invalid data. According to ASTM D638-14 section 5.1.3.3, coarse surface of the specimen on grip region is obtained via abrasive paper. In addition, the two-sided abrasive paper is located between specimen grip face and fixture clamp to prevent form slippage as seen in Figure 22a and 22b.

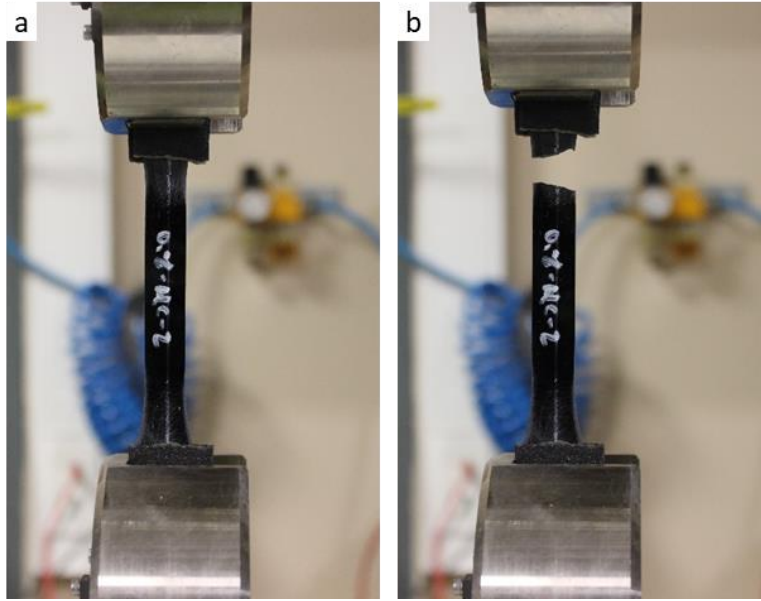


Figure 22: Tensile test fixture with specimen, a) before fracture b) after fracture

The stroke and load are recorded until the fracture occurs and the recorded maximum load is used to calculate the tensile strength, σ_t and tensile strain, ε_t values from,

$$\sigma_t = P/bd, \quad (3)$$

$$\varepsilon_t = D/L, \quad (4)$$

where, P is the maximum load in kN from the load displacement plot, b is the specimen width in mm, d is the specimen thickness in mm, D is maximum deflection of the specimen as maximum stroke of the crosshead, and L is distance between grips of 115 mm.

3.4. Dynamic Mechanical Analysis

The mechanical characterization of the specimens is performed using dynamic mechanical analysis (DMA) measuring system (Perkin Elmer DMA 8000 Dynamic Mechanical Analyzer) with a 3-point bending test specimen per ASTM D7028-07. The test method covers the procedure for the determination of the glass transition temperature of manufactured MWCNT reinforced polymer matrix composite under

flexural oscillation mode. The specimens have a length of 45 mm, width of 5 mm and thickness of 3 mm; giving a span-to-thickness ratio of 10:1. One specimen is tested for each material type.

The specimens are located on the test fixture as shown in Figure 23 by centering between clamps and fixed by hand. Due to the requirement of a mechanical testing of a polymer material according to the ASTM standard, the static test parameters are used. The frequency is set to the value of 1 Hz. Constant strain mode is operated at 0.05. The test run is programmed to start at 30°C close to room temperature and to terminate at an arranged DMA T_G of 180°C. The heating rate is 5°C/min; a thermocouple is located on the fixture close to the specimen. When the program reaches 30°C, the temperature holds for one minute and the data collection is commenced and is collected every 0.5 seconds. Storage modulus, tangent delta and T_G of the material are obtained from the analyses.



Figure 23: 3-point bending test fixture with located specimen for DMA

Resultant T_G values are dependent on the physical properties, type of measuring apparatus and the experimental parameters used. The determined T_G may not be the same as that reported by other measurement techniques on the same test specimen. Therefore, the results are investigated for the comparison of all manufactured specimens with different type of reinforcement nanomaterial with different weight fractions to the base epoxy material. The base epoxy material is tested firstly and obtained results are validated according to the material datasheet prior to the comparison.

CHAPTER 4

RESULTS AND DISCUSSION

In the first section, SEM images of all specimens with different weight fraction and with different reinforcement group are presented and discussed. The performed fracture toughness, flexural and tensile test results are presented and discussed.

4.1. SEM Images

Dispersion quality of the specimens is investigated by scanning electron microscopy. The investigation is performed on the surface of the specimens depending on the scanning method. Diamond saw is used to cut out a 5 mm cube from the specimen. Specimens are covered with bakelite for the ease of hold during polish process; the bakelite discs are made with 30 mm in diameter and 5 mm in thickness. Then, the surface corresponding to the transverse section is polished prior to microscopy. To provide electron flow, those discs are covered with gold-palladium of 2 nm thickness.

The pull-out nanotubes cannot be observed on the surface since the polish process is performed. To achieve structure observation of the nanotubes the specimens should be bathed with ammonia solvent for 24-48 hours or the specimen fracture surface should be chemically etched. The SEM images shows the clustering of MWCNTs in the epoxy.

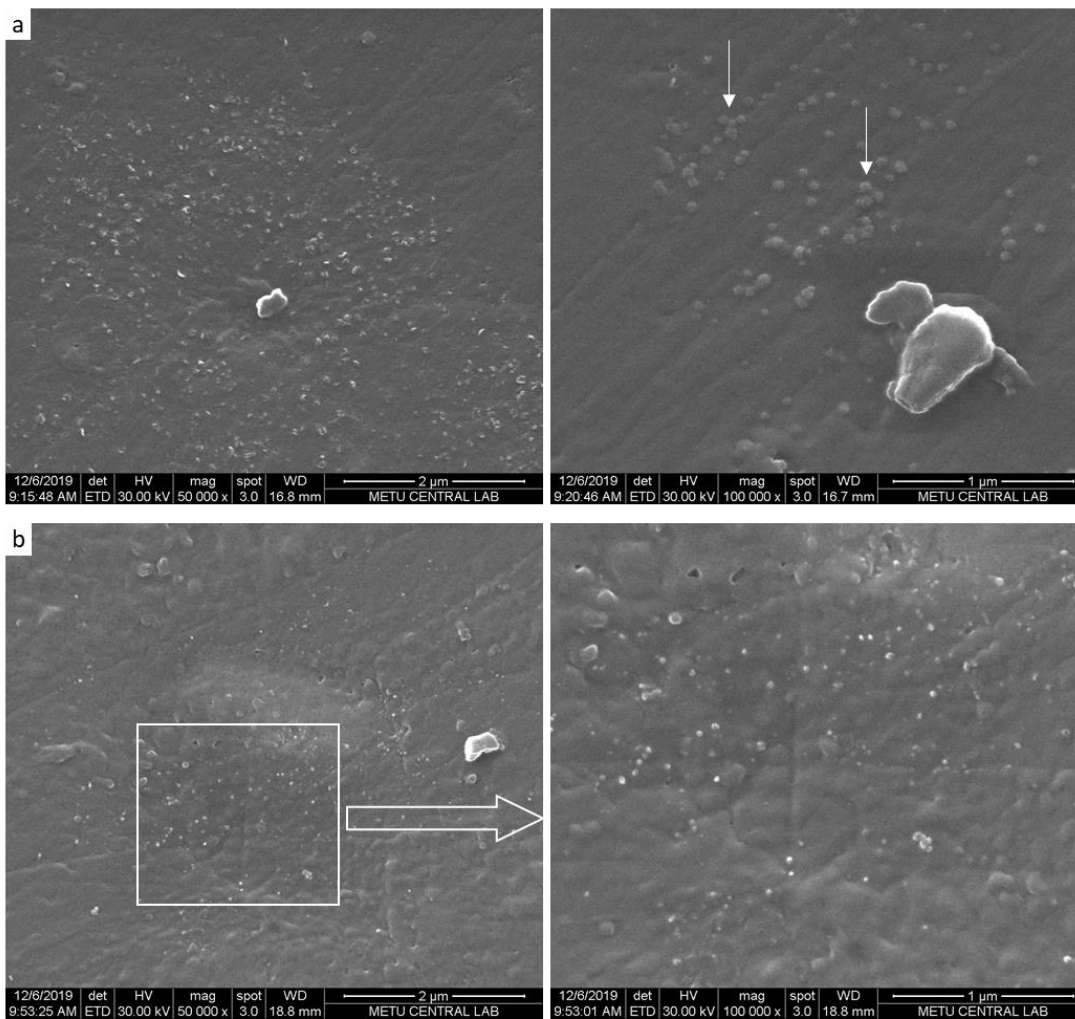


Figure 24: SEM images of 0.8 wt% MWCNT reinforced epoxy matrix composite a) with carboxyl-functionalized MWCNT reinforcement at 50,000x magnification (left), at 100,000x magnification (right); b) with non-functionalized MWCNT reinforcement at 50,000x magnification (left), at 100,000x magnification (right).

The achieved dispersion of 0.8 wt% carboxyl-functionalized MWCNT and non-functionalized MWCNT in the epoxy are compared in the SEM images in Figure 24a and 24b, respectively. Both types of nanomaterials are properly dispersed in the epoxy. Only some small agglomerates of 2-4 nanotubes are observed as pointed in Figure 24a and 24b.

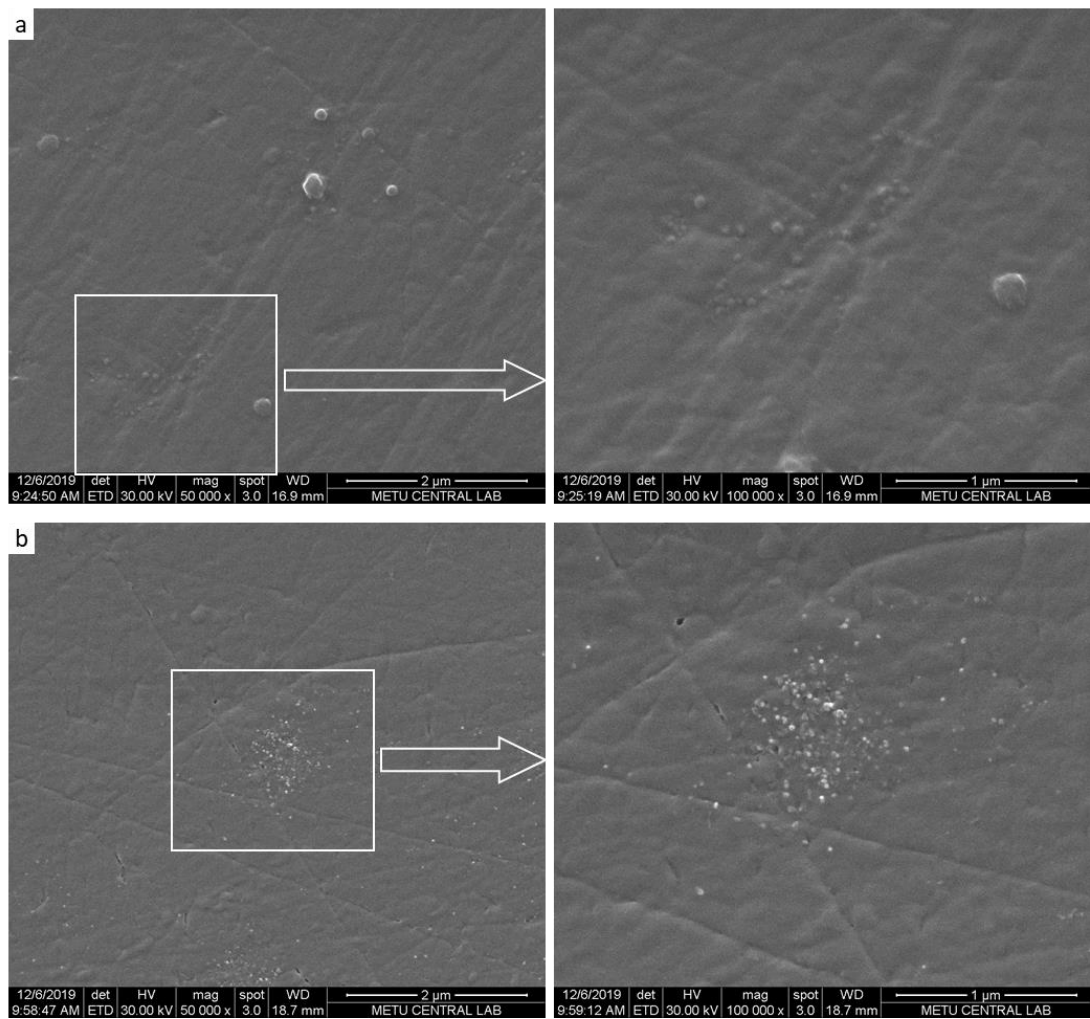


Figure 25: SEM images of 1.0 wt% MWCNT reinforced epoxy matrix composite a) with carboxyl-functionalized MWCNT reinforcement at 50,000x magnification (left), at 100,000x magnification (right); b) with non-functionalized MWCNT reinforcement at 50,000x magnification (left), at 100,000x magnification (right).

The agglomeration structure is similar for 0.8 wt% MWCNT-COOH reinforced epoxy (Figure 25a) and 1.0 wt% MWCNT-COOH; whereas, the agglomeration diameter increases to 1 μm and larger as seen in Figure 25b with increasing weight fraction of non-functionalized MWCNT.

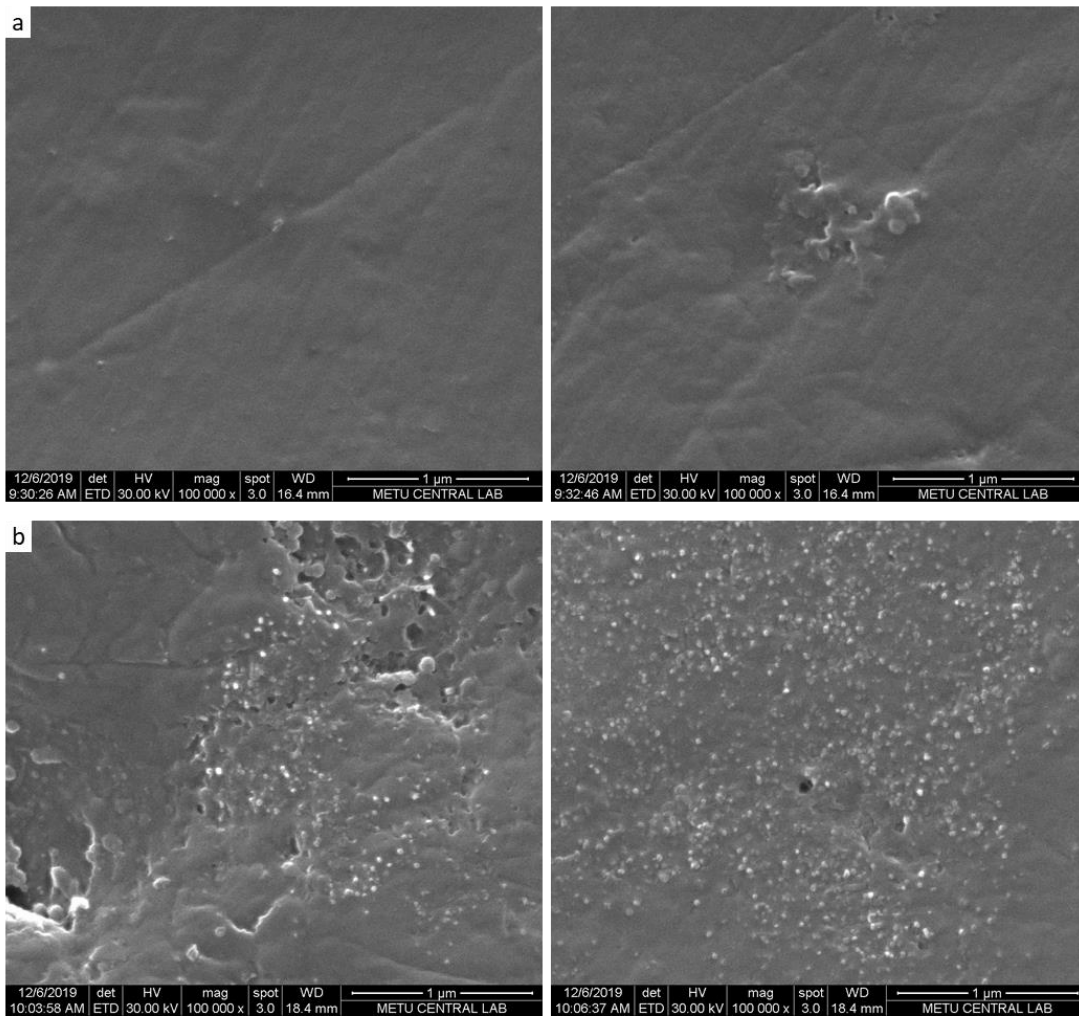


Figure 26: SEM images of 1.2 wt% MWCNT reinforced epoxy matrix composite a) with carboxyl-functionalized MWCNT reinforcement at 100,000x magnification; b) with non-functionalized MWCNT reinforcement at 100,000x magnification.

Figure 26 shows the 1.2 wt% MWCNT reinforced epoxy composite dispersion structure visualized by SEM. Carboxyl-functionalized MWCNT dispersion in the epoxy results with smoother surface in Figure 26a compared to non-functionalized MWCNT reinforcement. For the case of carboxyl-functionalized nanomaterial reinforcement, the polymer inhomogeneities are observed in the surface as bulk structure whether nanomaterial as seen in Figure 26a-right. However, for the case of non-functionalized nanomaterial reinforcement, the agglomerates of MWCNT are observed with diameter of 2 μm and higher in Figure 26b. The diameter of agglomeration of weight fraction of 1.2 is higher than that of 1.0.

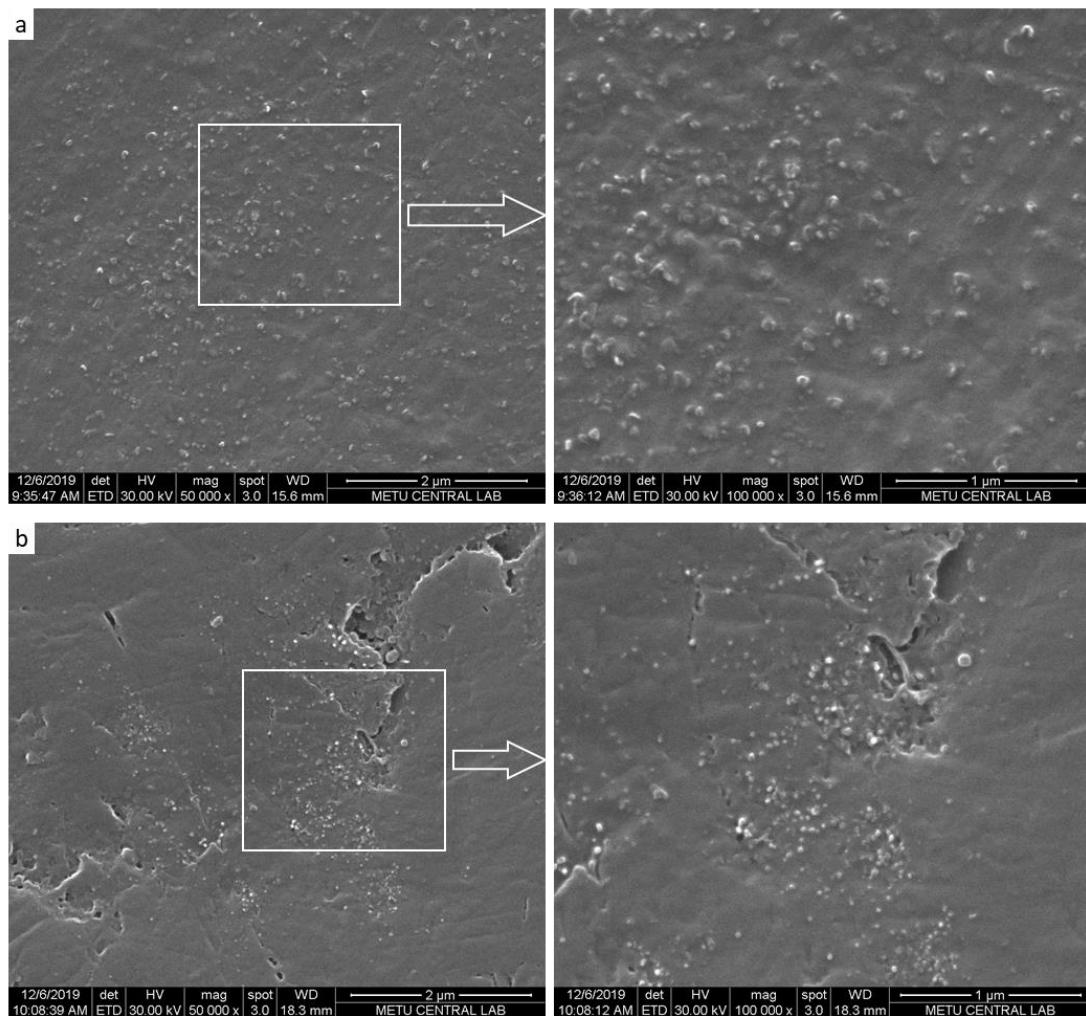


Figure 27: SEM images of 1.5 wt% MWCNT reinforced epoxy matrix composite a) with carboxyl-functionalized MWCNT reinforcement at 50,000x magnification (left), at 100,000x magnification (right); b) with non-functionalized MWCNT reinforcement at 50,000x magnification (left), at 100,000x magnification (right).

Increasing weight fraction of nanomaterial in the epoxy-based composite results with increasing agglomeration with entangled structure of MWCNT. Figure 27 shows the SEM images of MWCNT reinforcement with weight fraction of 1.5. Both chemical structure of nanomaterial results with enhancing agglomeration with increasing content in the epoxy as seen in Figure 27a and 27b. In the comparison of carboxyl-functionalized and non-functionalized MWCNT reinforcement effect in lower magnification, it is investigated that the nanomaterial with carboxyl-functionalization (Figure 27a-left) is well-dispersed in the epoxy whereas non-

functionalization of nanomaterial (Figure 27b-left) causes agglomeration of the nanomaterial and inhomogeneities.

4.2. Fracture Toughness

The experimental determination of the fracture toughness by SENB test method is performed on base and reinforced specimens. Figure 28 shows the load-displacement behavior of the SENB specimens for the same initial crack length of 1.0 cm. The curves are shown for carboxyl-functionalized MWCNT reinforcement at weight fraction of 0.8, 1.5 and 2.0% and for non-functionalized MWCNT reinforcement at weight fractions of 2.0%. The load increases linearly with displacement until the failure load is reached where the crack propagates unstably and divided the specimen into two parts. Carboxyl-functionalized MWCNT reinforced epoxy composite has the highest ultimate failure load at 0.8 of weight fraction; for weight fraction of 1.5 and 2.0% the failure load is almost the same. Non-functionalized MWCNT reinforced epoxy composite specimen with 2.0 wt% reaches a higher load at failure compared to all carboxyl-functionalized MWCNT reinforced specimens. K_{IC} values with corresponding initial crack lengths for all specimens are given in Appendix D1.

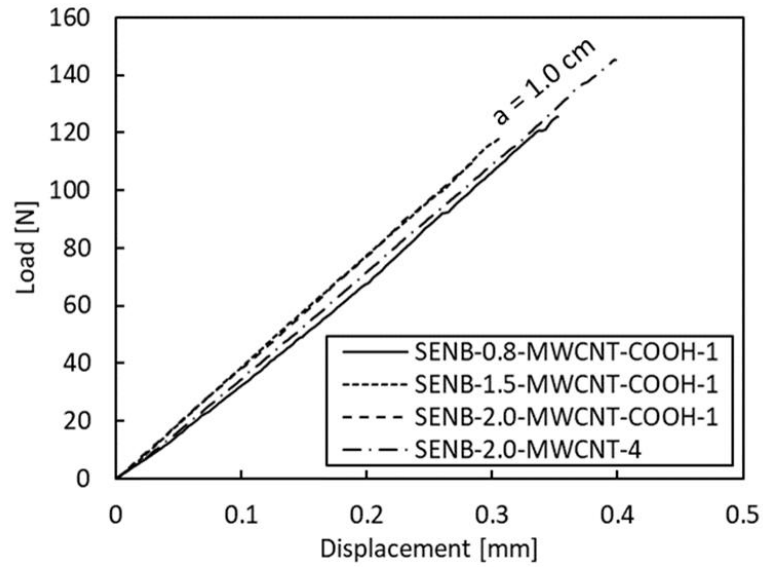


Figure 28: Load and displacement plot for initial crack length of 1.0 cm with $a/W = 0.4$

The load and displacement graphs for all tested specimens are given in Appendix E1. Using these load-displacement plots, the average fracture toughness and their deviations are calculated and shown in Figure 29. All nanocomposites have approximately the same fracture toughness with the neat epoxy ($K_{IC} = 1.01 \text{ MPa}\cdot\text{m}^{1/2}$). Experimentally calculated K_{IC} values ($0.9\text{-}1.1 \text{ MPa}\cdot\text{m}^{1/2}$) for the reinforced composite specimens are higher than polymer fracture toughness ($0.7\text{-}1.0 \text{ MPa}\cdot\text{m}^{1/2}$) consistent with the literature. A significant differences of fracture toughness, K_{IC} values between carboxyl-functionalized MWCNT and non-functionalized MWCNT compared to unreinforced matrix composite is not observed in the result of this study.

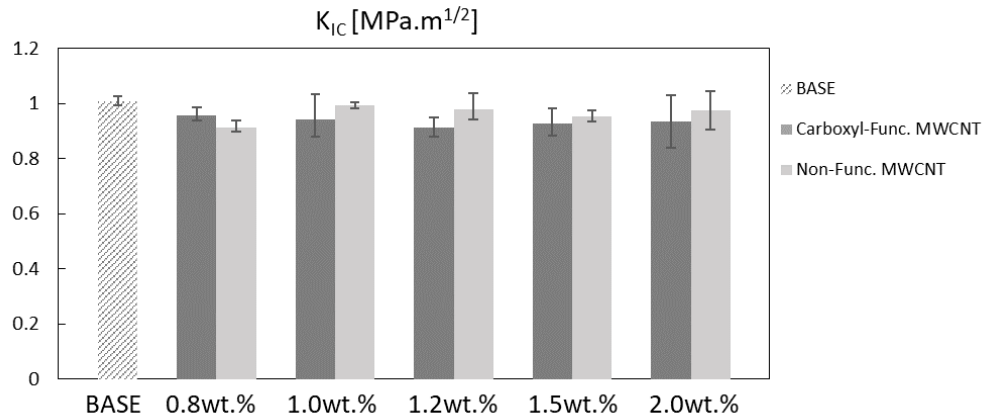


Figure 29: Fracture toughness of MWCNT reinforced epoxy matrix composite and base epoxy with different fractions

It is observed that fracture toughness is higher by 5% for 0.8 wt% MWCNT-COOH reinforcement compared to non-functionalized MWCNT one. In contrast, the fracture toughness is higher by 5% for 1.0, 1.2, 1.5 and 2.0 wt% non-functionalized MWCNT, in comparison to reinforcement of MWCNT-COOH. It can be explained by air voids that appeared during manufacturing process due to increasing dispersion viscosity with increasing CNT content. The air voids are more extensive on the surface and cross section of specimens with non-functionalized MWCNT reinforced composite at higher weight fractions; therefore, K_{IC} values are found to increase.

In one specimen reinforced with 1.5 wt% non-functionalized MWCNT (specimen SENB-1.5-NM-2), K_{IC} value of that specimen is calculated as 2.1 MPa.m^{1/2}, which is an increase by 100%. In Figure 30, the fracture surface of specimens with 1.5 wt% non-functionalized are shown; in Figure 30a, the standard fracture surface of a tested specimen is shown. In Figure 30b, at the fracture of the specimen, the propagation of the initial crack is arrested at the location where an air bubble is located. Subsequent to further loading, a new crack initializes and propagates until the specimen separates into two parts. The value is excluded for the average K_{IC} of 1.5 wt% reinforcement of non-functionalized MWCNT.

The crack propagation path depends on the material porosity in the preparation procedure of specimen for test fixture of SENB. When the crack front propagates unstably and stops at porosity, to advance the crack, higher stress is needed for further propagation as discussed by Romhányi et al. [32].

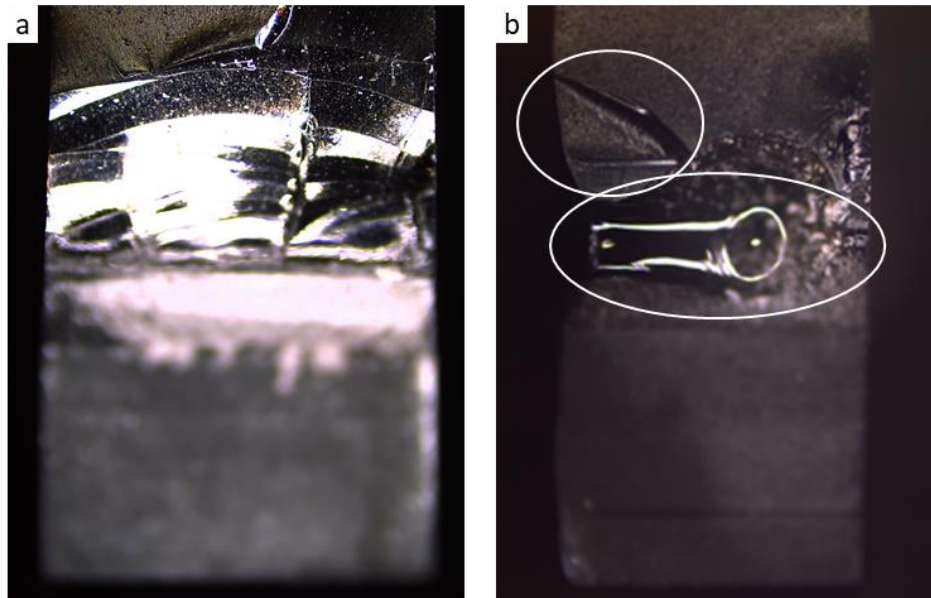


Figure 30: 1.5 wt% non-functionalized MWCNT reinforced epoxy specimens a) standard fracture surface, b) fracture surface with air bubbles

In the fracture toughness experiments, the crack growth occurs unstably and the crack path is not a straight line. When the load reaches the maximum level, the fracture is instantaneous. The crack path is not observed as linear because the porosity is higher for non-functionalized MWCNT reinforced epoxy composite. For the compared fractions the crack growth surfaces are very similar.

4.3. Flexural Strength

Figure 31 shows representative flexural stress vs. strain curves for COOH-MWCNT and non-functionalized MWCNT reinforced composite material. The plots show the different weight fractions for both cases in addition to base material. For all

cases, it is seen that the strain to failure decreases with respect to the base material. The flexural strength is found to increase only for weight fraction of 2.0% for carboxyl-functionalized MWCNT compared to the base material. The strength rose from 424 MPa to 476 MPa. For lower weight percentages, the functionalized specimens have almost the same strength as the base material.

In contrast, the flexural strength is found to increase for 0.8 wt% non-functionalized specimen (from 424 MPa to 465 MPa). For higher weight fractions of non-functionalized reinforcement, the flexural strength degrades by 25% for 1.2 wt% reinforcement and by 75% for 2.0 wt% reinforcement. The failure strain for 2.0 wt% reinforcement also drops significantly (almost by 50%). The flexural stress vs. strain values and curves for all tested materials are presented in Appendix D2 and E2.

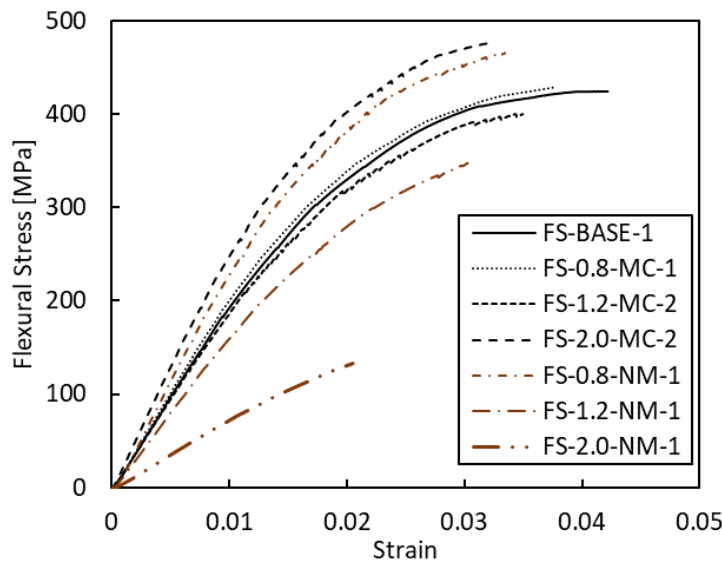


Figure 31: Flexural stress-strain curves of MWCNT reinforced epoxy matrix composite and base epoxy with different fractions

The flexural strengths for all the specimens are shown in Figure 32 where mean values are shown as columns and the deviations are shown as error bars. The strength value of each fraction is compared with base material. For carboxyl-functionalized nanomaterial, flexural strength is found to increase with weight fractions above 1.2% for all specimens in each test group. In contrast, the flexural strength decreases with

increasing weight fraction for non-functionalized nanomaterial. The strength of non-functionalized MWCNT reinforced epoxy is found to increase for 0.8 wt% by 12.5% and then decreases for higher weight fractions greater than 1.0 wt%. Again at 2.0 wt% reinforcement of non-functionalized MWCNT, there is a significant degradation in flexural strength by 75% compared to base material.

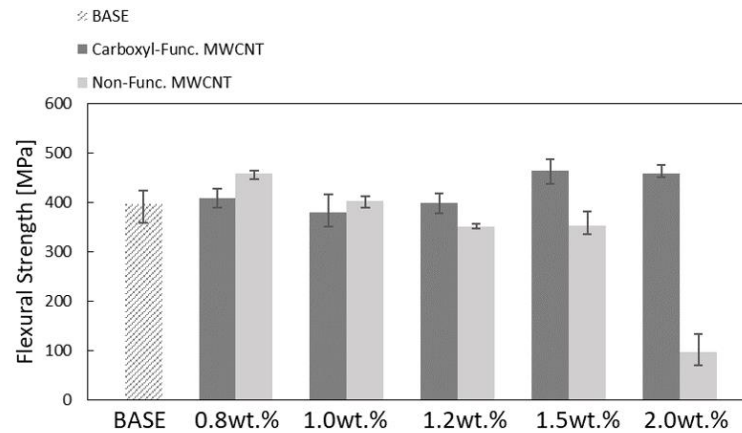


Figure 32: Flexural strength of MWCNT reinforced epoxy matrix composite and base epoxy with different fractions

The addition of carboxyl-functionalized MWCNT to epoxy polymer increases the flexural strength by 17% compared to neat epoxy for specimens with weight fraction higher than 1.2%. In contrast, in the case of non-functionalized MWCNT addition, flexural strength improves by 15% compared to neat epoxy for specimens with weight fraction lower than 1.0.

4.4. Tensile Strength

Figure 33 shows representative tensile stress vs. strain curves for COOH-MWCNT and non-functionalized MWCNT reinforced composite material. Ultimate tensile strength and strain of specimens are determined from the P_{max} value. The curves are shown for different weight fractions for both cases in addition to base material. The curves are very similar to each other with differing maximum stresses and failure strains. The failure strain value is higher than base material for 0.8 wt% carboxyl-functionalized MWVCNT reinforcement; whereas, in all the other cases the failure strain is lower. The failure load for 2.0 wt% non-functionalized MWCNT reinforced

epoxy composite is the lowest of all under tensile loading. All the specimens have higher stiffness than base material except 0.8 wt.% functionalized-MWCNT reinforcement. Tensile strength and corresponding strain values for all tested specimens are given in Appendix D3.

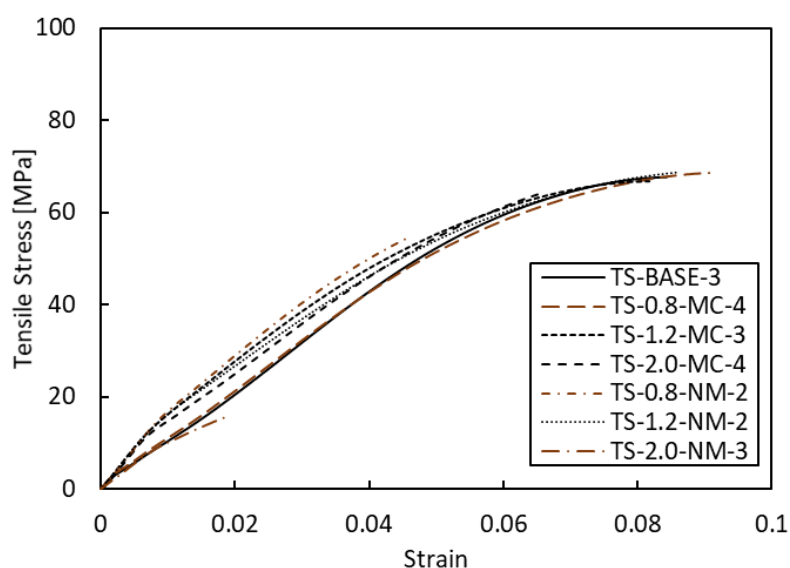


Figure 33: Tensile properties of MWCNT reinforced epoxy matrix composite and base epoxy with different fractions

Figure 34 presents the tensile strength of reinforced composites for each fraction and base material. Carboxyl-functionalized and non-functionalized nanomaterial reinforcement effects are compared with the base material.

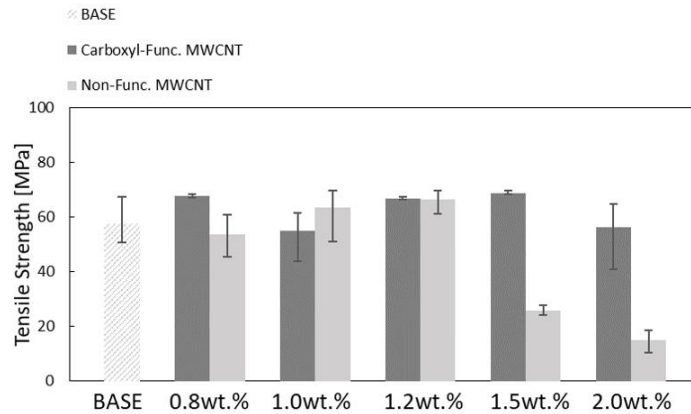


Figure 34: Tensile strength of MWCNT reinforced epoxy matrix composite and base epoxy with different fractions

It is observed that measured tensile strength of specimens with 0.8, 1.2 and 1.5 wt% carboxyl-functionalized MWCNT reinforcement are higher by 15% compared to the base material. For weight fraction of 1.0 and 2.0%, the tensile strength is found to degrade by 17% compared the base material.

Non-functionalized MWCNT reinforced specimens have lower tensile strength for weight fraction of 0.8 by 7% compared to base material. For weight fractions of 1.0 and 1.2%, the tensile strength is increased by 16%. However, the tensile strength decreases significantly by 74% for higher weight fractions of 1.5 and 2.0% compared to base material.

4.5. Dynamic Mechanical Analysis

The viscoelastic properties of the nanocomposites are presented in Figure 35; storage modulus of functionalized and non-functionalized MWCNT reinforced epoxy matrix composites are compared. There is not a remarkable effect of nanomaterial reinforcement on storage modulus of nanocomposite material compared to the neat epoxy.

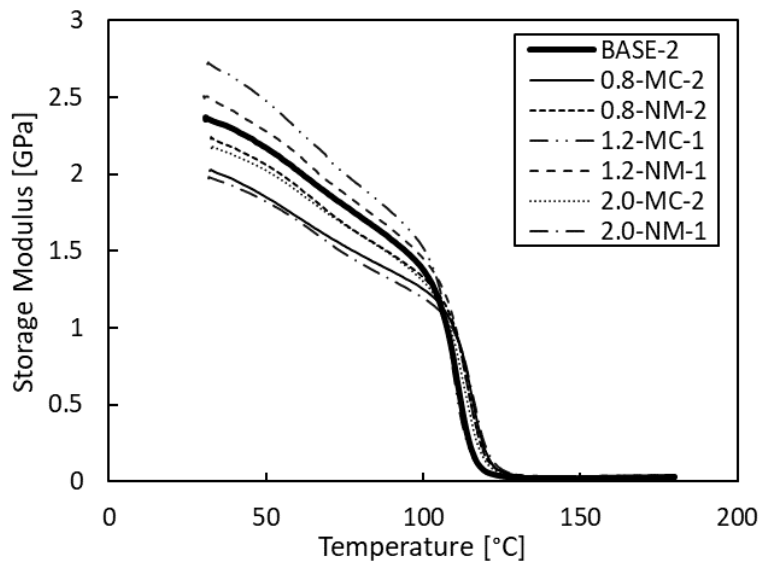


Figure 35: Storage modulus of non-functionalized and carboxyl-functionalized MWCNT reinforced epoxy matrix composite and base epoxy with different fractions

Tan delta represents the damping ratio of the nanocomposites. It is expected to increase with increasing weight fraction of nanomaterial in the epoxy-based composite. However, in Figure 36, it is observed that weight fraction of MWCNT from 0.8 to 2.0 and functionalization of reinforcement nanomaterial do not affect the tan delta values measured with increasing temperature.

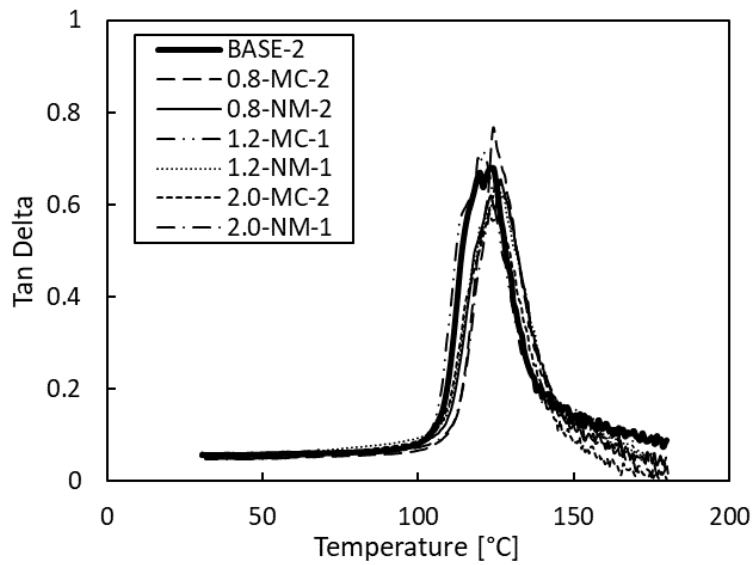


Figure 36: Tan delta of non-functionalized and carboxyl-functionalized MWCNT reinforced epoxy matrix composite and base epoxy with different fractions

Functionalization of the CNTs improved the glass transition temperature of the epoxy composites, and CNT-OH showed 34% enhancement in T_G which is the highest one from other CNT reinforcement and base material in the study of Roy et al. [21]. In contrast to the study of Roy, the T_G of nanomaterial reinforced epoxy composite material is compared with the base material in Figure 37. The resultant T_G remains almost constant with variance of MWCNT content.

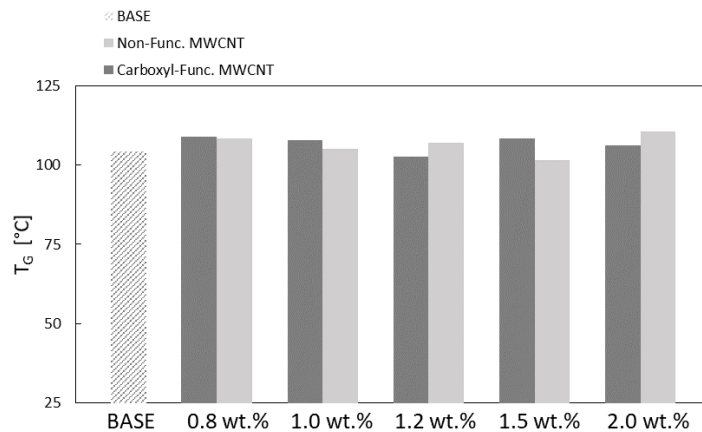


Figure 37: Glass transition temperature of non-functionalized and carboxyl-functionalized MWCNT reinforced epoxy matrix composite and base epoxy with different fractions

CHAPTER 5

CONCLUSION

In this work, the effect of MWCNT reinforcement on the mechanical properties of epoxy matrix composites has been studied. The standard calender technique by three-roll mill machine is applied in order to disperse multi-wall nanotubes in the epoxy resin with shear forcing. The epoxy matrix nanocomposites are reinforced with carboxyl-functionalized MWCNT and non-functionalized MWCNT in different weight fractions of 0.8, 1.0, 1.2, 1.5 and 2.0. The specimens are manufactured by curing in vacuum oven on molding tools. The manufactured nanocomposites are investigated by mechanical tests and scanning electron microscopy in order to determine toughness, strength and to observe achieved dispersion of CNT and epoxy resin.

The use of three-roll mill machine is an appropriate technique to disperse CNT in epoxy. The efficiency of this technique is not limited to the laboratory scale; the method could be effective for the production of composite parts. Carboxyl-functionalized MWCNT dispersion process is more applicable than that of non-functionalized MWCNT for weight fractions of higher than 1.2%.

The polymer epoxy does not have molecular attraction with carboxyl functionalization group. Therefore, the dispersion viscosity is lower with the reinforcement of functionalized-MWCNT and the agglomeration is higher since the nanomaterial is not wet by matrix.

Dispersion of non-functionalized MWCNT into epoxy with 2.0% weight fraction is impractical via three-roll mill. Furthermore, the surface quality of epoxy matrix composites reinforced with this fraction of non-functionalized MWCNT is not acceptable to manufacture composite parts due to the air bubbles that could not be removed during curing. The reason for those is the high viscosity of the dispersion.

The settled fraction where mechanical properties start to degrade is much lower than 4.0% which is reported as the fraction where the agglomeration starts and air bubbles emerge in the study of Tarfaoui et al. [19]. For lower CNT weight fractions, the cure process should be optimized by arranging the vacuum period to eliminate the interphase porosity structure and air bubbles and to improve the surface quality.

The fracture toughness of the composites does not increase at CNT content by 2.0 wt% compared to the base epoxy. In contrast to Gojny et al. [11], according to SENB tests, carbon nanotube filling of the epoxy at low weight fractions does not have a beneficial effect on the toughness. This is independent of the type of filler.

The addition of small amounts of CNT leads to improved mechanical properties. In comparison to base epoxy material, CNT reinforced epoxy matrix composite shows an increased tensile strength by 20% and 15% and flexural strength by 17% and 15% for filler material type of MWCNT-COOH and non-functionalized MWCNT, relatively, for lower weight fractions than 1.5%.

The storage modulus of the CNT reinforced composite material does not have remarkable change compared to the base material. Similarly, T_G values in different weight fractions are nearly the same with base material, according to the DMA measurements.

Addition of higher weight fractions than 2.0 for MWCNT-COOH is expected to decrease the strength and fracture toughness because of CNT being tend to agglomerate. For the fractions used in the study, a further increase of the mechanical properties of MWCNT reinforced epoxy matrix composites can be expected by a variation of the processing parameters. The calendaring parameters can be changed to increase the dispersion quality of non-functionalized MWCNT in the epoxy.

REFERENCES

- [1] O'Donnell, S. E., Sprong, K. R., Haltli, B. M. (2004). Potential Impact of Carbon Nanotube Reinforced Polymer Composite on Commercial Aircraft Performance and Economics. *AIAA 4th Aviation Technology, Integration and Operation Forum*, 1–10.
- [2] Khan, S. U., & Kim, J. K. (2011). Impact and delamination failure of multiscale carbon nanotube-fiber reinforced polymer composites: A review. *International Journal of Aeronautical and Space Sciences*, 12(2), 115–133. <https://doi.org/10.5139/IJASS.2011.12.2.115>
- [3] Thostenson, E. T., Ren, Z., & Chou, T. (2001). *Advances in the science and technology of carbon nanotubes and their composites: a review*. 61, 1899–1912. [https://doi.org/10.1016/S0266-3538\(01\)00094-X](https://doi.org/10.1016/S0266-3538(01)00094-X)
- [4] Arash, B., Wang, Q., & Varadan, V. K. (2014). Mechanical properties of carbon nanotube/polymer composites. *Scientific Reports*, 4, 1–8. <https://doi.org/10.1038/srep06479>
- [5] Arca, M. A., & Coker, D. (2014). Experimental investigation of CNT effect on curved beam strength and interlaminar fracture toughness of CFRP laminates. *Journal of Physics: Conference Series*, 524(1). <https://doi.org/10.1088/1742-6596/524/1/012038>
- [6] Safadi, B., Andrews, R., & Grulke, E. A. (2002). Multiwalled carbon nanotube polymer composites: Synthesis and characterization of thin films. *Journal of Applied Polymer Science*, 84(14), 2660–2669. <https://doi.org/10.1002/app.10436>
- [7] Tibbetts, G. G., & McHugh, J. J. (1999). Mechanical properties of vapor-grown carbon fiber composites with thermoplastic matrices. *Journal of Materials Research*, 14(7), 2871–2880. <https://doi.org/10.1557/JMR.1999.0383>
- [8] Ma, P. C., Siddiqui, N. A., Marom, G., & Kim, J. K. (2010). Dispersion and functionalization of carbon nanotubes for polymer-based nanocomposites: A review. *Composites Part A: Applied Science and Manufacturing*, 41(10), 1345–1367. <https://doi.org/10.1016/j.compositesa.2010.07.003>
- [9] Schadler, L. S., Giannaris, S. C., & Ajayan, P. M. (1998). Load transfer in carbon nanotube epoxy composites. *Applied Physics Letters*, 73(26), 3842–3844. <https://doi.org/10.1063/1.122911>

- [10] Lu, J. P. (1997). Elastic properties of single and multilayered nanotubes. *Journal of Physics and Chemistry of Solids*, 58(11), 1649–1652. [https://doi.org/10.1016/S0022-3697\(97\)00045-0](https://doi.org/10.1016/S0022-3697(97)00045-0)
- [11] Gojny, F. H., Wichmann, M. H. G., Köpke, U., Fiedler, B., & Schulte, K. (2004). Carbon nanotube-reinforced epoxy-composites: Enhanced stiffness and fracture toughness at low nanotube content. *Composites Science and Technology*, 64(15 SPEC. ISS.), 2363–2371. <https://doi.org/10.1016/j.compscitech.2004.04.002>
- [12] Thostenson, E. T., & Chou, T. W. (2006). Processing-structure-multi-functional property relationship in carbon nanotube/epoxy composites. *Carbon*, 44(14), 3022–3029. <https://doi.org/10.1016/j.carbon.2006.05.014>
- [13] Yang, C. K., Lee, Y. R., Hsieh, T. H., Chen, T. H., & Cheng, T. C. (2018). Mechanical property of multiwall carbon nanotube reinforced polymer composites. *Polymers and Polymer Composites*, 26(1), 99–104. <https://doi.org/10.1177/096739111802600112>
- [14] Kumar, P., & Srinivas, J. (2019). Study on mechanical and viscoelastic behavior of carbon nanotube (CNT) reinforced Epofine1564 nanocomposite. 29(4), 13–22. <https://doi.org/10.14456/jmmm.2019.42>
- [15] A, P. P., Rajamohan, V., & Mathew, A. T. (2019). Material and Mechanical Characterization of Multi-Functional Carbon Nanotube Reinforced Hybrid Composite Materials. *Experimental Techniques*, 43(3), 301–314. <https://doi.org/10.1007/s40799-019-00316-0>
- [16] Quan, D., Urdániz, J. L., & Ivanković, A. (2018). Enhancing mode-I and mode-II fracture toughness of epoxy and carbon fibre reinforced epoxy composites using multi-walled carbon nanotubes. *Materials and Design*, 143, 81–92. <https://doi.org/10.1016/j.matdes.2018.01.051>
- [17] Moaseri, E., Bazubandi, B., Baniadam, M., & Maghrebi, M. (2019). Enhancement in mechanical properties of multiwalled carbon nanotube-reinforced epoxy composites: Crosslinking of the reinforcement with the matrix via diamines. *Polymer Engineering and Science*, 59(9), 1905–1910. <https://doi.org/10.1002/pen.25191>
- [18] Fadhil, B. M., Ahmed, P. S., & Kamal, A. A. (2016). Improving mechanical properties of epoxy by adding multi-wall carbon nanotube. *Journal of Theoretical and Applied Mechanics (Poland)*, 54(2), 551–560. <https://doi.org/10.15632/jtam-pl.54.2.551>

- [19] Tarfaoui, M., Lafdi, K., & El Moumen, A. (2016). Mechanical properties of carbon nanotubes based polymer composites. *Composites Part B: Engineering*, 103, 113–121. <https://doi.org/10.1016/j.compositesb.2016.08.016>
- [20] Cha, J., Jin, S., Shim, J. H., Park, C. S., Ryu, H. J., & Hong, S. H. (2016). Functionalization of carbon nanotubes for fabrication of CNT/epoxy nanocomposites. *Materials and Design*, 95, 1–8. <https://doi.org/10.1016/j.matdes.2016.01.077>
- [21] Roy, S., Petrova, R. S., & Mitra, S. (2018). Effect of carbon nanotube (CNT) functionalization in epoxy-CNT composites. *Nanotechnology Reviews*, 7(6), 475–485. <https://doi.org/10.1515/ntrev-2018-0068>
- [22] Ehsan Moaseri, Bazubandi, B., Karimi, M., Maghrebi, M., & Baniadam, M. (2019). Mechanical Improvements of Multi-Walled Carbon Nanotube-Epoxy Composite: Covalent Functionalization of Multi-Walled Carbon Nanotube by Epoxy Chains. *Polymer Science - Series B*, 61(3), 341–348. <https://doi.org/10.1134/S1560090419030072>
- [23] Wang, L., Tan, Y., Wang, X., Xu, T., Xiao, C., & Qi, Z. (2018). Mechanical and fracture properties of hyperbranched polymer covalent functionalized multiwalled carbon nanotube-reinforced epoxy composites. *Chemical Physics Letters*, 706, 31–39. <https://doi.org/10.1016/j.cplett.2018.05.07>
- [24] Iijima, S. (1991). Helical microtubules of graphitic carbon. *Nature*, 354, 56–58.
- [25] Srivastava, D., Wei, C., & Cho, K. (2003). Nanomechanics of carbon nanotubes and composites. *Applied Mechanics Reviews*, 56(2), 215. <https://doi.org/10.1115/1.1538625>
- [26] Hassanzadeh-aghdam, M. K., Ansari, R., & Darvizeh, A. (2018). Micromechanical analysis of carbon nanotube-coated fiber-reinforced hybrid composites. *International Journal of Engineering Science*, 130, 215–229. <https://doi.org/10.1016/j.ijengsci.2018.06.001>
- [27] Yakobson, Boris I., Avouris, P. (2001). Mechanical properties of carbon nanotubes. *Topics Appl. Phys.*, 80(2001), 287–327.
- [28] Qian, D., Wagner, G. J., Liu, W. K., Yu, M.-F., & Ruoff, R. S. (2002). Mechanics of carbon nanotubes. *Applied Mechanics Reviews*, 55(6), 495–553. <https://doi.org/10.1115/1.1490129>
- [29] Xu, L. R., Bhamidipati, V., Zhong, W. H., Li, J., Lukehart, C. M., Lara-Curzio, E., Lance, M. J. (2004). Mechanical property characterization of a polymeric

nanocomposite reinforced by graphitic nanofibers with reactive linkers. *Journal of Composite Materials*, 38(18), 1563–1582. <https://doi.org/10.1177/0021998304043758>

- [30] Shaffer, M. S. P., Fan, X., & Windle, A. H. (1998). Dispersion and packing of carbon nanotubes. *Carbon*, 36(11), 1603–1612. [https://doi.org/10.1016/S0008-6223\(98\)00130-4](https://doi.org/10.1016/S0008-6223(98)00130-4)
- [31] Frankland, S. J. V, Caglar, A., Brenner, D. W., & Griebel, M. (2002). Molecular Simulation of the Influence of Chemical Cross-Links on the Shear Strength of. *Journal of Physical Chemistry B*, 106(12), 3046–3048.
- [32] Romhány, G., & Szabó, G. (2009). Interlaminar crack propagation in MWCNT/fiber reinforced hybrid composites. *Express Polymer Letters*, 3(3), 145–151. <https://doi.org/10.3144/expresspolymlett.2009.19>

APPENDICES

A. CNT Reinforced Epoxy Polymer Composite Specimen Data per ASTM Standards

Varying CNT Weight Fraction and Functionalized CNT Type Effect on Resin																	
test standard	width [mm]	length [mm]	thickness [mm]	initial crack length [mm]	resin density [g/cm ³]	CNT weight %	FUNC CNT weight %	CNT density [g/cm ³]	specimen number	specimen number per plate	plate width [mm]	plate length [mm]	plate qty	total resin qty [CM]	total resin qty [g]	total CNT qty [g]	total FUNC CNT qty [g]
SENB ASTM D5045 (GIC)	25,0±0,2	110±1	6,5	12,5±1,0	1,2	0,8%	0,0%	2,4	3	6	230	140	1	0,0002093	251,16	2,025484	0
	25,0±0,2	110±1	6,5	12,5±1,0	1,2	1,0%	0,0%	2,4	3	6	230	140	1	0,0002093	251,16	2,53697	0
	25,0±0,2	110±1	6,5	12,5±1,0	1,2	1,2%	0,0%	2,4	3	6	230	140	1	0,0002093	251,16	3,050526	0
	25,0±0,2	110±1	6,5	12,5±1,0	1,2	1,5%	0,0%	2,4	3	6	230	140	1	0,0002093	251,16	3,824772	0
	25,0±0,2	110±1	6,5	12,5±1,0	1,2	2,0%	0,0%	2,4	3	6	230	140	1	0,0002093	251,16	5,125714	0
	25,0±0,2	110±1	6,5	12,5±1,0	1,2	0,0%	0,8%	2,4	3	6	230	140	1	0,0002093	251,16	0	2,025484
	25,0±0,2	110±1	6,5	12,5±1,0	1,2	0,0%	1,0%	2,4	3	6	230	140	1	0,0002093	251,16	0	2,53697
	25,0±0,2	110±1	6,5	12,5±1,0	1,2	0,0%	1,2%	2,4	3	6	230	140	1	0,0002093	251,16	0	3,050526
	25,0±0,2	110±1	6,5	12,5±1,0	1,2	0,0%	1,5%	2,4	3	6	230	140	1	0,0002093	251,16	0	3,824772
ASTM D5045 (GIC) BASE	25,0±0,2	110±1	6,5	12,5±1,0	1,2	0,0%	0,0%	2,4	3	6	230	140	1	0,0002093	251,16	0	5,125714
	25,0±0,2	110±1	6,5	12,5±1,0	1,2	0,0%	0,0%	2,4	3	6	230	140	1	0,0002093	251,16	0	5,125714
Flexural Strength of Polymers ASTM D790	12,5±0,2	125±1	3	-	1,2	0,8%	0,0%	2,4	5	10	245	155	1	0,0001139	136,71	1,1025	0
	12,5±0,2	125±1	3	-	1,2	1,0%	0,0%	2,4	5	10	245	155	1	0,0001139	136,71	1,380909	0
	12,5±0,2	125±1	3	-	1,2	1,2%	0,0%	2,4	5	10	245	155	1	0,0001139	136,71	1,660445	0
	12,5±0,2	125±1	3	-	1,2	1,5%	0,0%	2,4	5	10	245	155	1	0,0001139	136,71	2,081878	0
	12,5±0,2	125±1	3	-	1,2	2,0%	0,0%	2,4	5	10	245	155	1	0,0001139	136,71	2,79	0
	12,5±0,2	125±1	3	-	1,2	0,0%	0,8%	2,4	5	10	245	155	1	0,0001139	136,71	0	1,1025
	12,5±0,2	125±1	3	-	1,2	0,0%	1,0%	2,4	5	10	245	155	1	0,0001139	136,71	0	1,380909
	12,5±0,2	125±1	3	-	1,2	0,0%	1,2%	2,4	5	10	245	155	1	0,0001139	136,71	0	1,660445
	12,5±0,2	125±1	3	-	1,2	0,0%	1,5%	2,4	5	10	245	155	1	0,0001139	136,71	0	2,081878
ASTM D790 BASE	12,5±0,2	125±1	3	-	1,2	0,0%	0,0%	2,4	5	10	245	155	1	0,0001139	136,71	0	2,79
Tensile Strength of Polymers ASTM D638	19,0±0,5	165±1	5	-	1,2	0,8%	0,0%	2,4	5	10	310	195	1	0,0003023	362,7	2,925	0
	19,0±0,5	165±1	5	-	1,2	1,0%	0,0%	2,4	5	10	310	195	1	0,0003023	362,7	3,663636	0
	19,0±0,5	165±1	5	-	1,2	1,2%	0,0%	2,4	5	10	310	195	1	0,0003023	362,7	4,405263	0
	19,0±0,5	165±1	5	-	1,2	1,5%	0,0%	2,4	5	10	310	195	1	0,0003023	362,7	5,52335	0
	19,0±0,5	165±1	5	-	1,2	2,0%	0,0%	2,4	5	10	310	195	1	0,0003023	362,7	7,402041	0
	19,0±0,5	165±1	5	-	1,2	0,0%	0,8%	2,4	5	10	310	195	1	0,0003023	362,7	0	2,925
	19,0±0,5	165±1	5	-	1,2	0,0%	1,0%	2,4	5	10	310	195	1	0,0003023	362,7	0	3,663636
	19,0±0,5	165±1	5	-	1,2	0,0%	1,2%	2,4	5	10	310	195	1	0,0003023	362,7	0	4,405263
	19,0±0,5	165±1	5	-	1,2	0,0%	1,5%	2,4	5	10	310	195	1	0,0003023	362,7	0	5,52335
	19,0±0,5	165±1	5	-	1,2	0,0%	2,0%	2,4	5	10	310	195	1	0,0003023	362,7	0	7,402041
	ASTM D638 BASE	19,0±0,5	165±1	5	-	1,2	0,0%	0,0%	2,4	5	10	310	195	1	0,0003023	362,7	0

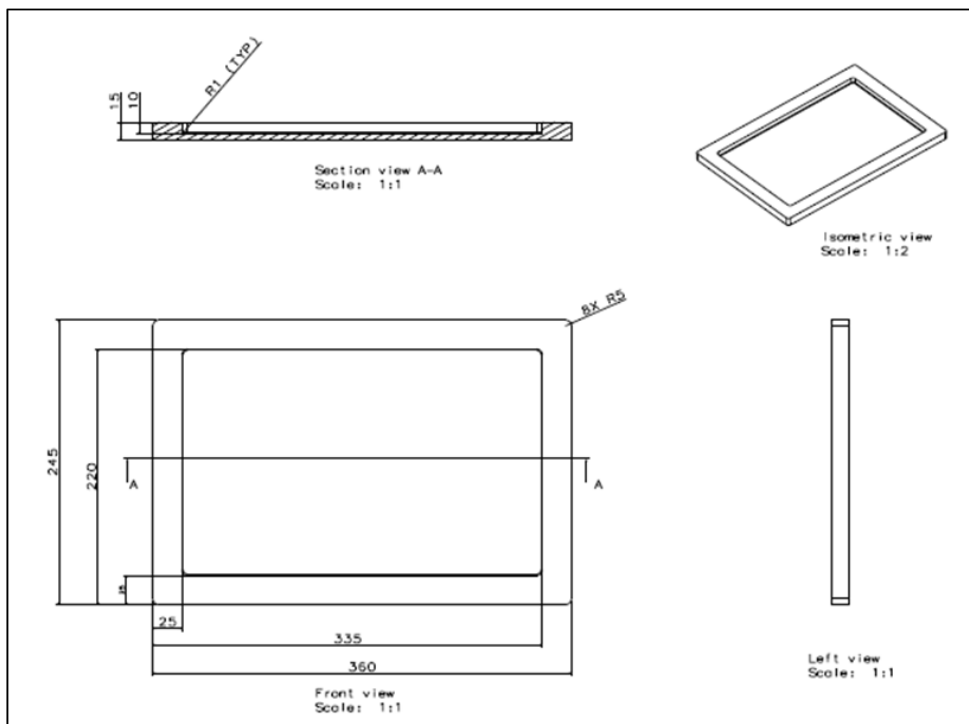
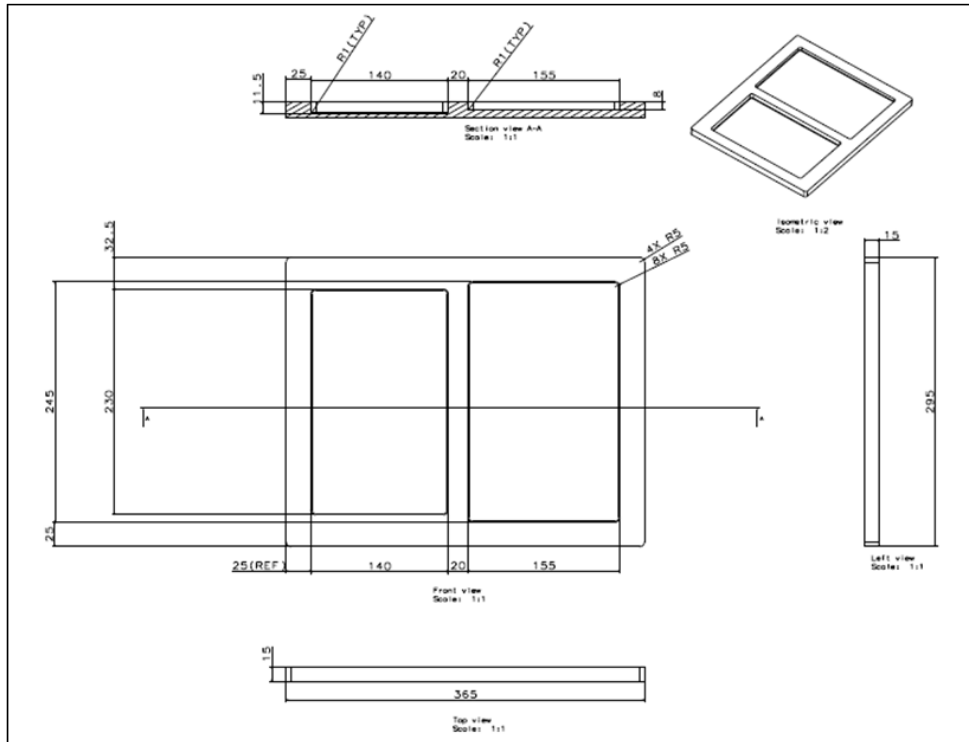
B. MWCNT/Epoxy Polymer Dispersion by Three-Roll Mill Data

CNT type	Epoxy qty [gr]	CNT percentage	CNT qty [gr]	Date	Cycle number	Speed [rpm]	Duration [min]	Total duration [min]	Photo taken	Final weight [gr]	Weight fraction [gr]	Total final weight [gr]
MWCNT-COOH	350	0,80%	2,80	24.06.2019	first	20	30	96	1	348	-4,80	697
					second	25	12		-			
					third	25	12		-			
					fourth	28	12		-			
					fifth	28	11		1			
					sixth	30	10		-			
					seventh	35	9		1			
	350	0,80%	2,80	24.06.2019	first	20	17	75	-	349	-3,80	
					second	25	12		1			
					third	28	10		-			
					fourth	28	10		-			
					fifth	30	9		1			
					sixth	30	9		-			
					seventh	35	8		-			
MWCNT-COOH	400	1,00%	4,00	25.06.2019	first	20	20	85	1	405	1,00	809
					second	25	13		-			
					third	25	13		1			
					fourth	28	11		-			
					fifth	30	10		1			
					sixth	30	9		-			
					seventh	30	9		1			
	400	1,00%	4,00	25.06.2019	first	20	20	97	-	404	0,00	
					second	20	20		-			
					third	25	13		-			
					fourth	28	14		-			
					fifth	28	12		-			
					sixth	30	10		-			
					seventh	35	8		-			
MWCNT-COOH	400	1,20%	4,80	26.06.2019	first	20	23	113	-	402	-2,80	807
					second	20	23		1			
					third	25	16		1			
					fourth	25	16		1			
					fifth	28	13		-			
					sixth	30	12		1			
					seventh	35	10		1			
	400	1,20%	4,80	26.06.2019	first	20	25	115	2	405	0,20	
					second	20	25		1			
					third	25	18		1			
					fourth	25	15		1			
					fifth	28	12		1			
					sixth	30	11		1			
					seventh	35	9		1			
MWCNT-COOH	400	1,50%	6,00	27.06.2019	first	20	28	126	2	398	-8,00	806
					second	20	29		2			
					third	25	18		2			
					fourth	25	17		2			
					fifth	28	14		2			
					sixth	30	11		2			
					seventh	35	9		2			
	400	1,50%	6,00	27.06.2019	first	20	30	141	2	408	2,00	
					second	20	30		2			
					third	25	20		2			
					fourth	25	22		2			
					fifth	28	16		2			
					sixth	30	13		2			
					seventh	35	10		2			
MWCNT-COOH	400	2,00%	8,00	28.06.2019	first	20	28	124	1	406	-2,00	817
					second	20	32		1			
					third	25	15		1			
					fourth	25	15		1			
					fifth	28	13		1			
					sixth	30	11		1			
					seventh	35	10		1			
	400	2,00%	8,00	28.06.2019	first	20	23	114	1	411	3,00	
					second	20	26		1			
					third	25	16		1			
					fourth	25	16		1			
					fifth	28	12		1			
					sixth	30	11		1			
					seventh	35	10		1			

CNT type	Epoxy qty [gr]	CNT percentage	CNT qty [gr]	Date	Cycle number	Speed [rpm]	Duration [min]	Total duration [min]	Photo taken	Final weight [gr]	Weight fraction [gr]	Total final weight [gr]
MWCNT	400	0,80%	3,20	01.07.2019	first	20	19	79	2	393	-10,20	796
					second	20	16		1			
					third	25	9		1			
					fourth	25	10		1			
					fifth	28	8		1			
					sixth	30	10		-			
					seventh	35	7		-			
	400	0,80%	3,20	01.07.2019	first	20	25	83	1	403	-0,20	
					second	20	17		1			
					third	25	10		1			
					fourth	25	10		1			
					fifth	28	8		1			
					sixth	30	7		1			
					seventh	35	6		1			
MWCNT	400	1,00%	4,00	03.07.2019	first	20	16	62	1	398	-6,00	805
					second	20	14		1			
					third	25	8		1			
					fourth	25	8		1			
					fifth	28	6		1			
					sixth	30	5		1			
					seventh	35	5		1			
	400	1,00%	4,00	03.07.2019	first	20	20	80	1	407	3,00	
					second	20	28		1			
					third	25	8		2			
					fourth	25	7		1			
					fifth	28	6		1			
					sixth	30	6		1			
					seventh	35	5		1			
MWCNT	400	1,20%	4,80	04.07.2019	first	20	23	75	1	404	-0,80	812
					second	20	19		1			
					third	25	8		-			
					fourth	25	8		1			
					fifth	28	6		1			
					sixth	30	6		1			
					seventh	35	5		1			
	400	1,20%	4,80	04.07.2019	first	20	21	68	2	408	3,20	
					second	20	16		1			
					third	25	7		1			
					fourth	25	7		1			
					fifth	28	6		1			
					sixth	30	6		1			
					seventh	35	5		1			
MWCNT	400	1,50%	6,00	05.07.2019	first	20	24	77	2	395	-11,00	798
					second	20	14		1			
					third	25	8		1			
					fourth	25	8		1			
					fifth	28	8		1			
					sixth	30	7		1			
					seventh	35	8		1			
	400	1,50%	6,00	05.07.2019	first	20	21	67	2	403	-3,00	
					second	20	13		1			
					third	25	8		1			
					fourth	25	8		1			
					fifth	28	6		1			
					sixth	30	6		1			
					seventh	35	5		1			
MWCNT	400	2,00%	8,00	05.07.2019	first	20	21	77	2	406	-2,00	809
					second	20	17		1			
					third	25	8		1			
					fourth	25	9		1			
					fifth	28	8		1			
					sixth	30	7		1			
					seventh	35	7		1			
	400	2,00%	8,00	05.07.2019	first	20	20	77	1	403	-5,00	
					second	20	16		1			
					third	25	8		1			
					fourth	25	10		1			
					fifth	28	8		1			
					sixth	30	7		1			
					seventh	35	8		1			

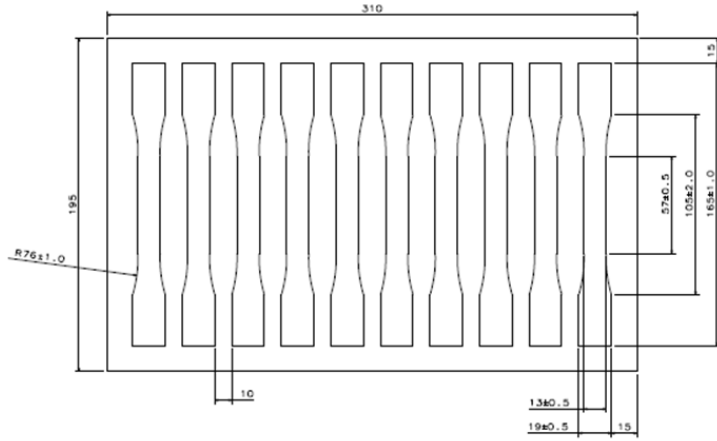
C. Manufacturing Data

C1. Designed Casting Tool

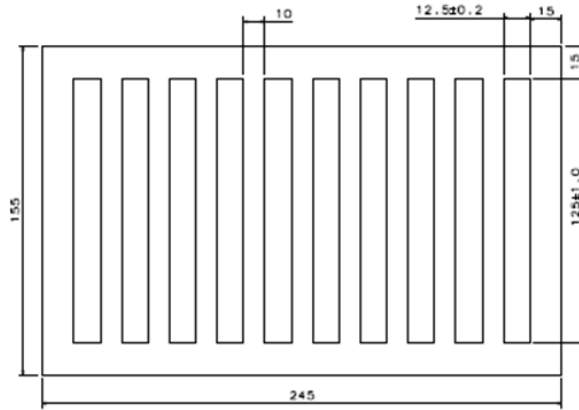


C2. Specimen Routing Data

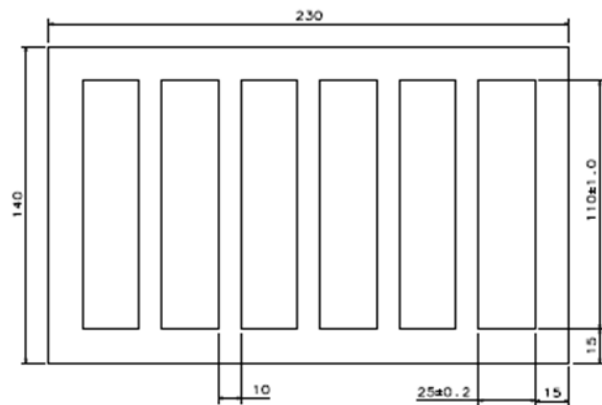
SPECIMEN ROUTING PER ASTM D638-14



SPECIMEN ROUTING PER ASTM D790-03



SPECIMEN ROUTING PER ASTM D5045-14



D. Raw Test Data

D1. SENB Fracture Toughness Test

G _{ic} Specimen Name	a-initial [cm]	P _{max} [kN]	d _{max} [mm]	K _{ic} [MPa. m ^{1/2}]
SENB-BASE-1	0.670	0.197	0.631	1.028
SENB-BASE-2	1.301	0.091	0.419	0.994
SENB-BASE-3	0.658	0.167	0.545	1.007
SENB-0.8-MC-1	1.013	0.131	0.392	0.945
SENB-0.8-MC-2	0.576	0.222	0.412	0.939
SENB-0.8-MC-3	0.772	0.169	0.433	0.988
SENB-1.0-MC-1	1.389	0.069	0.397	0.880
SENB-1.0-MC-2	1.221	0.086	0.459	0.906
SENB-1.0-MC-3	0.739	0.155	0.425	1.035
SENB-1.2-MC-2	0.731	0.134	0.319	0.949
SENB-1.2-MC-3	1.286	0.048	0.352	0.910
SENB-1.2-MC-4	0.684	0.118	0.330	0.880
SENB-1.5-MC-1	1.034	0.119	0.324	0.982
SENB-1.5-MC-2	0.739	0.163	0.325	0.884
SENB-1.5-MC-3	0.845	0.145	0.332	0.913
SENB-2.0-MC-1	1.003	0.114	0.364	0.937
SENB-2.0-MC-2	1.776	0.030	0.474	0.839
SENB-2.0-MC-3	0.816	0.146	0.380	1.030
SENB-0.8-NM-1	0.686	0.149	0.360	0.937
SENB-0.8-NM-2	1.440	0.061	0.355	0.897
SENB-0.8-NM-3	1.519	0.053	0.376	0.908
SENB-1.0-NM-1	0.642	0.173	0.397	0.981
SENB-1.0-NM-3	1.142	0.102	0.436	1.004
SENB-1.2-NM-1	0.876	0.129	0.369	1.036
SENB-1.2-NM-2	1.222	0.084	0.361	0.943
SENB-1.2-NM-3	0.747	0.140	0.427	0.957
SENB-1.5-NM-1	0.841	0.120	0.412	0.975
SENB-1.5-NM-3	0.650	0.181	0.496	1.265
SENB-1.5-NM-4	1.134	0.076	0.353	0.934
SENB-2.0-NM-1	0.915	0.196	0.513	1.043
SENB-2.0-NM-2	0.682	0.219	0.415	0.905
SENB-2.0-NM-4	1.033	0.152	0.456	0.975

D2. Flexural Tests

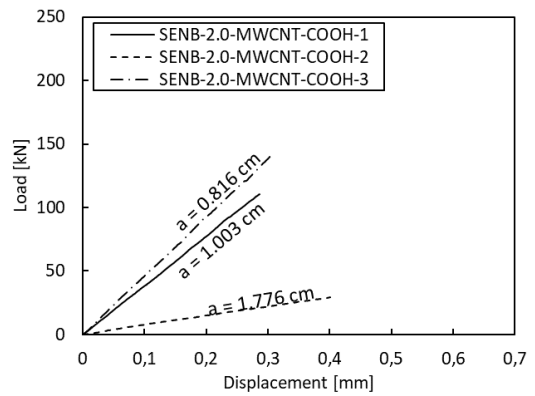
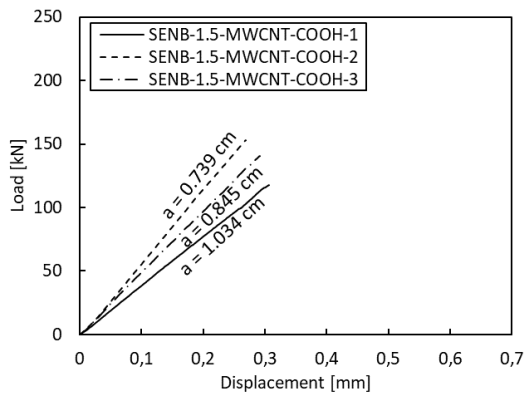
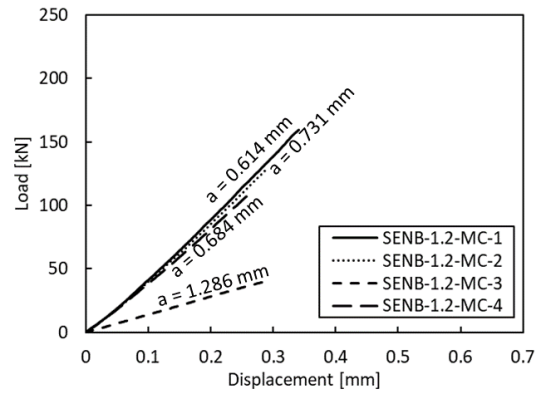
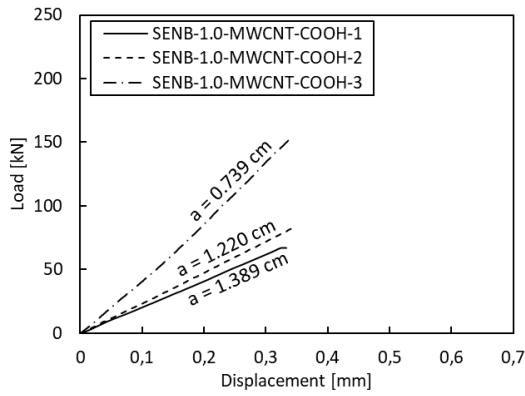
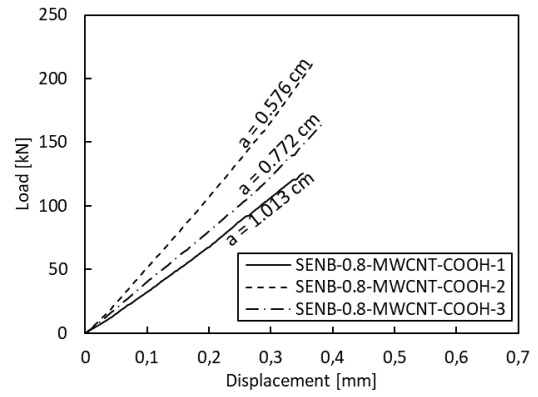
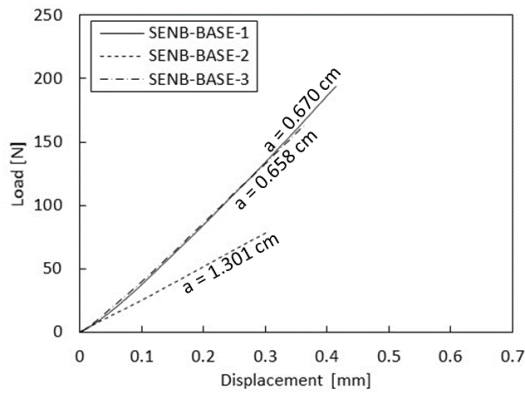
Flexural Strength Specimen Name	Pmax [N]	Dmax [mm]	Flexural Strength [Mpa]	Flexural Strain
FS-BASE-1	1059.9	5.970	424.468	0.042
FS-BASE-2	1082.0	5.737	410.368	0.042
FS-BASE-3	818.6	2.986	359.618	0.020
FS-0.8-MC-1	995.8	5.538	428.927	0.038
FS-0.8-MC-2	993.7	4.447	389.928	0.032
FS-0.8-MC-3	855.3	3.916	404.852	0.025
FS-1.0-MC-1	1151.9	5.456	371.977	0.043
FS-1.0-MC-2	1024.8	3.973	350.505	0.030
FS-1.0-MC-3	945.1	4.872	417.249	0.033
FS-1.2-MC-1	1037.8	4.610	378.224	0.034
FS-1.2-MC-2	1015.5	4.912	400.051	0.035
FS-1.2-MC-3	982.2	5.198	417.624	0.036
FS-1.5-MC-1	858.0	4.124	438.244	0.026
FS-1.5-MC-2	854.3	5.063	486.906	0.030
FS-1.5-MC-3	725.2	3.670	469.337	0.020
FS-2.0-MC-1	929.6	4.877	451.190	0.031
FS-2.0-MC-2	898.2	5.265	476.017	0.032
FS-2.0-MC-3	753.3	3.783	451.607	0.022
FS-0.8-NM-1	916.7	5.339	465.368	0.033
FS-0.8-NM-2	931.6	5.359	462.420	0.034
FS-0.8-NM-3	768.7	3.809	447.418	0.022
FS-1.0-NM-1	988.0	4.595	405.491	0.032
FS-1.0-NM-2	1003.3	5.626	412.778	0.039
FS-1.0-NM-3	924.5	4.470	390.247	0.031
FS-1.2-NM-1	1030.8	3.941	347.557	0.030
FS-1.2-NM-2	1051.1	4.259	357.479	0.033
FS-1.2-NM-3	1027.1	4.490	348.250	0.035
FS-1.5-NM-1	566.2	3.902	337.995	0.023
FS-1.5-NM-2	579.0	4.915	381.860	0.027
FS-1.5-NM-3	557.3	3.408	336.550	0.020
FS-2.0-NM-1	559.1	2.239	132.957	0.021
FS-2.0-NM-2	291.9	1.510	70.566	0.014
FS-2.0-NM-3	346.6	1.766	86.332	0.016

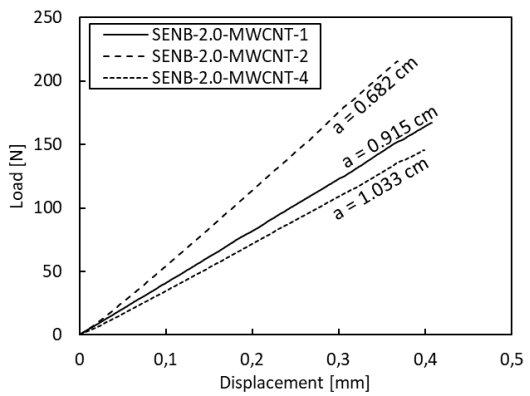
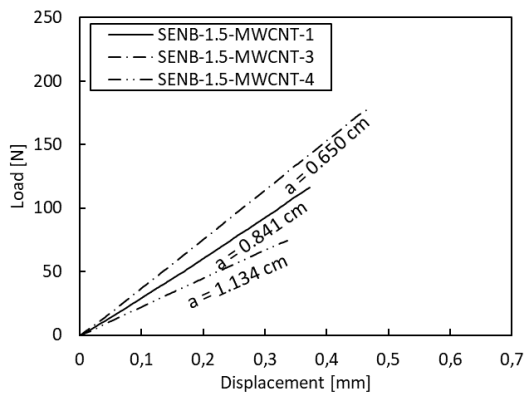
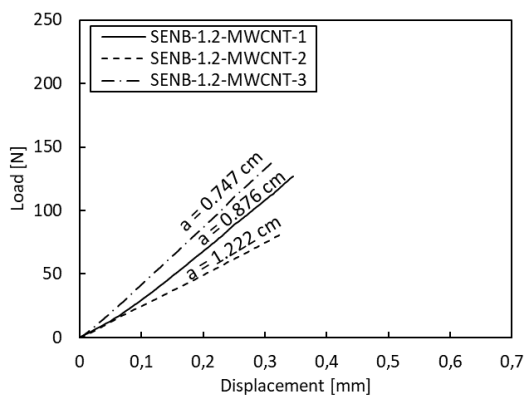
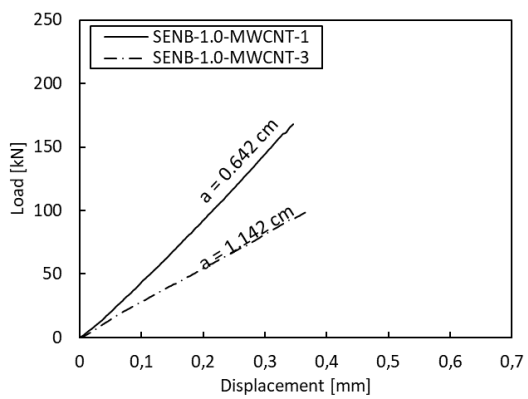
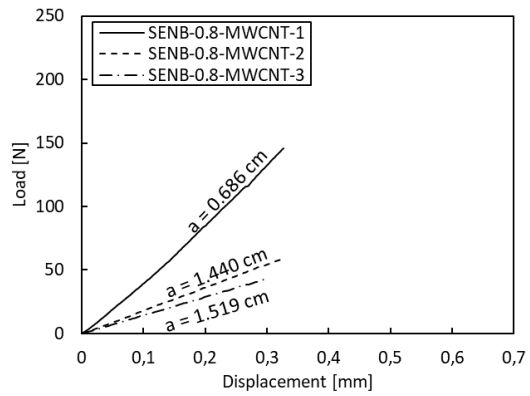
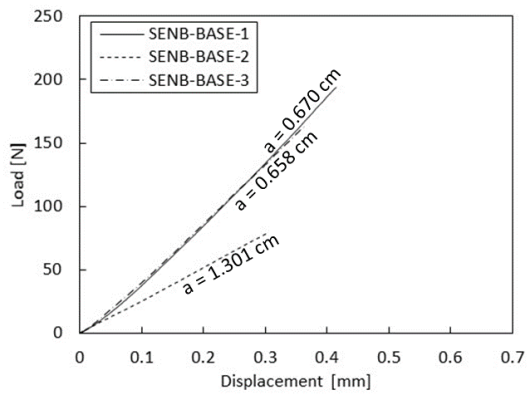
D3. Tensile Tests

Tensile Strength Specimen Name	Pmax [N]	Strokemax [mm]	Tensile Strength [Mpa]	Strain
TS-BASE-DNM	3616.0	3.644	54.179	0.032
TS-BASE-3	4265.5	9.696	67.608	0.084
TS-BASE-7	2853.2	4.853	50.910	0.042
TS-0.8-MC-2	4085.0	10.225	67.916	0.089
TS-0.8-MC-3	3647.1	9.069	67.051	0.079
TS-0.8-MC-4	4441.0	10.427	68.538	0.091
TS-1.0-MC-1	3207.5	6.612	61.673	0.057
TS-1.0-MC-2	2065.7	3.796	43.771	0.033
TS-1.0-MC-3	3478.5	6.351	60.028	0.055
TS-1.2-MC-1	4522.0	9.436	67.404	0.082
TS-1.2-MC-2	4401.5	9.603	66.632	0.084
TS-1.2-MC-3	4290.5	9.400	66.733	0.082
TS-1.5-MC-1	5053.0	11.007	68.542	0.096
TS-1.5-MC-2	4732.0	10.537	68.499	0.092
TS-1.5-MC-4	5038.5	10.138	69.850	0.088
TS-2.0-MC-2	2489.0	4.326	40.830	0.038
TS-2.0-MC-3	4412.5	7.631	64.892	0.066
TS-2.0-MC-4	4287.5	7.485	63.858	0.065
TS-0.8-NM-2	3471.8	5.330	54.882	0.046
TS-0.8-NM-3	2812.0	3.832	45.551	0.033
TS-0.8-NM-4	3832.5	6.612	60.904	0.057
TS-1.0-NM-2	4502.0	9.343	69.680	0.081
TS-1.0-NM-3	3436.1	5.230	51.204	0.045
TS-1.0-NM-4	4637.5	10.359	69.598	0.090
TS-1.2-NM-1	4259.0	7.243	61.440	0.063
TS-1.2-NM-2	4442.5	9.897	68.672	0.086
TS-1.2-NM-3	5021.0	10.280	69.804	0.089
TS-1.5-NM-1	1632.3	2.177	24.174	0.019
TS-1.5-NM-2	1577.7	2.489	25.201	0.022
TS-1.5-NM-3	1914.5	3.195	27.911	0.028
TS-2.0-NM-1	841.6	1.147	10.479	0.010
TS-2.0-NM-2	1617.5	2.927	18.724	0.025
TS-2.0-NM-3	1301.7	2.181	15.805	0.019

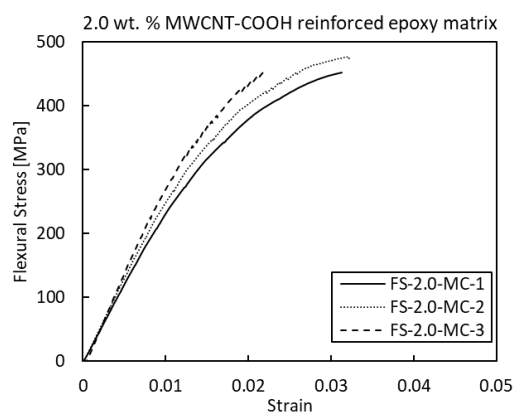
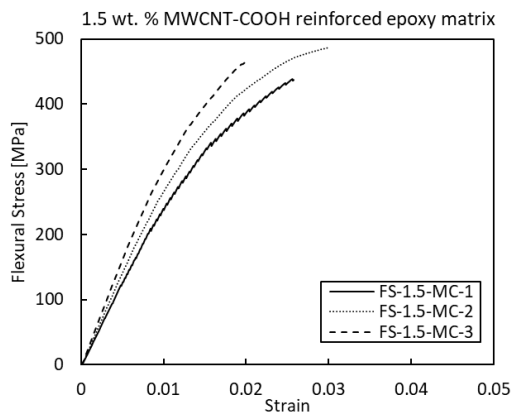
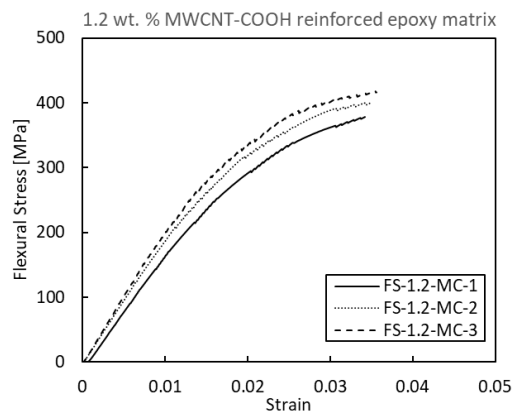
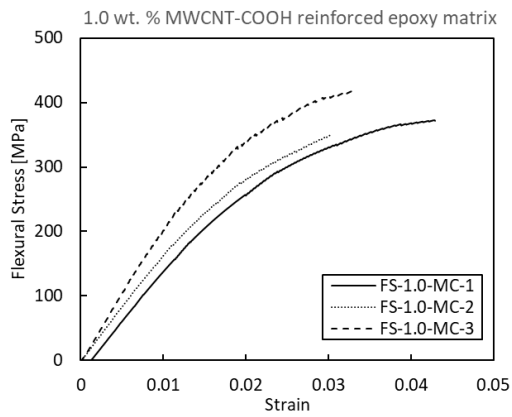
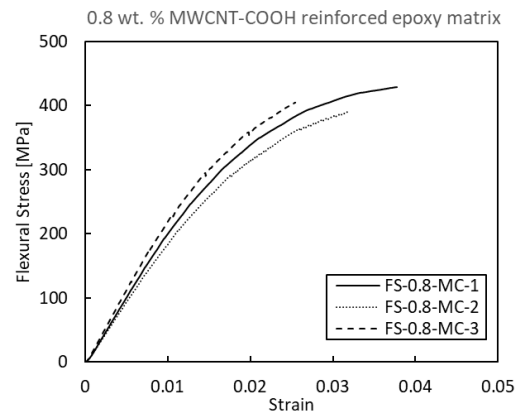
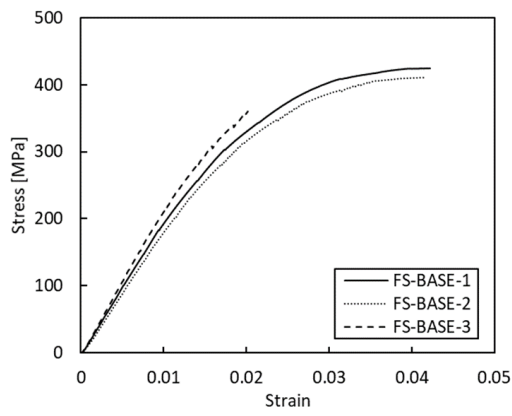
E. Graphed Test Results

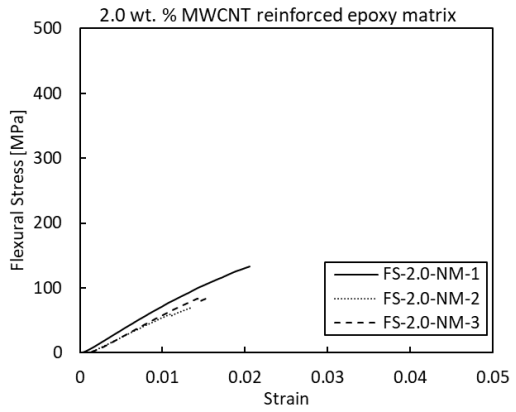
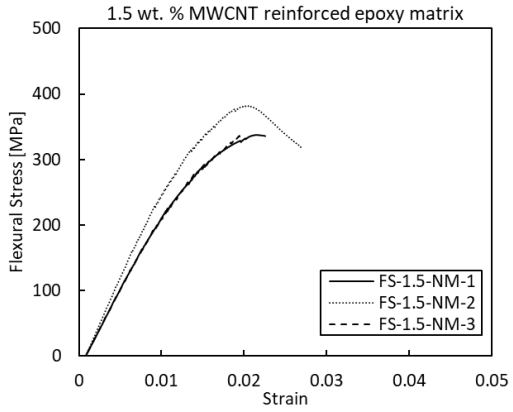
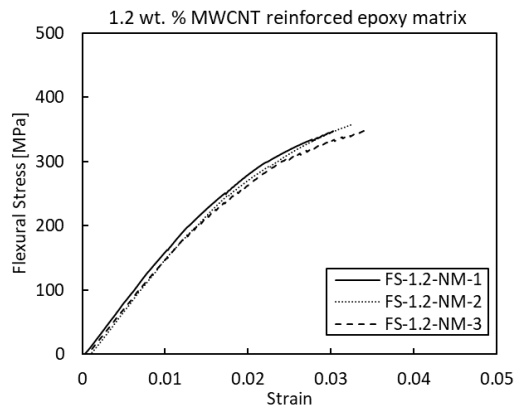
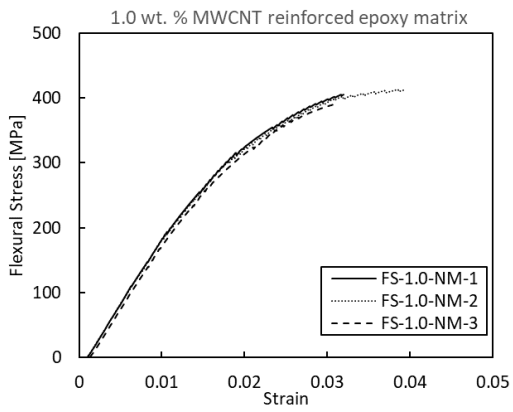
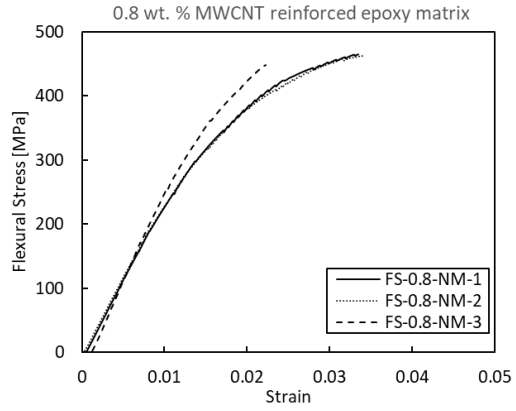
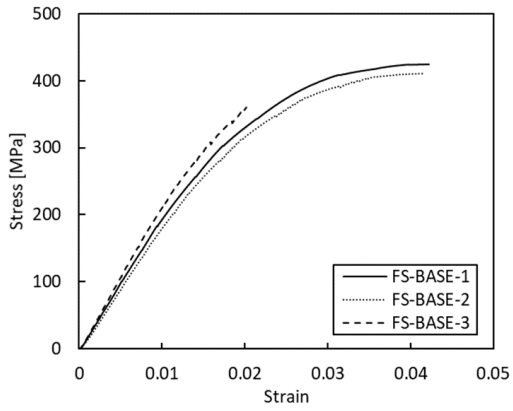
E1. Load and Displacement Plots for SEN(B) Fracture Tests



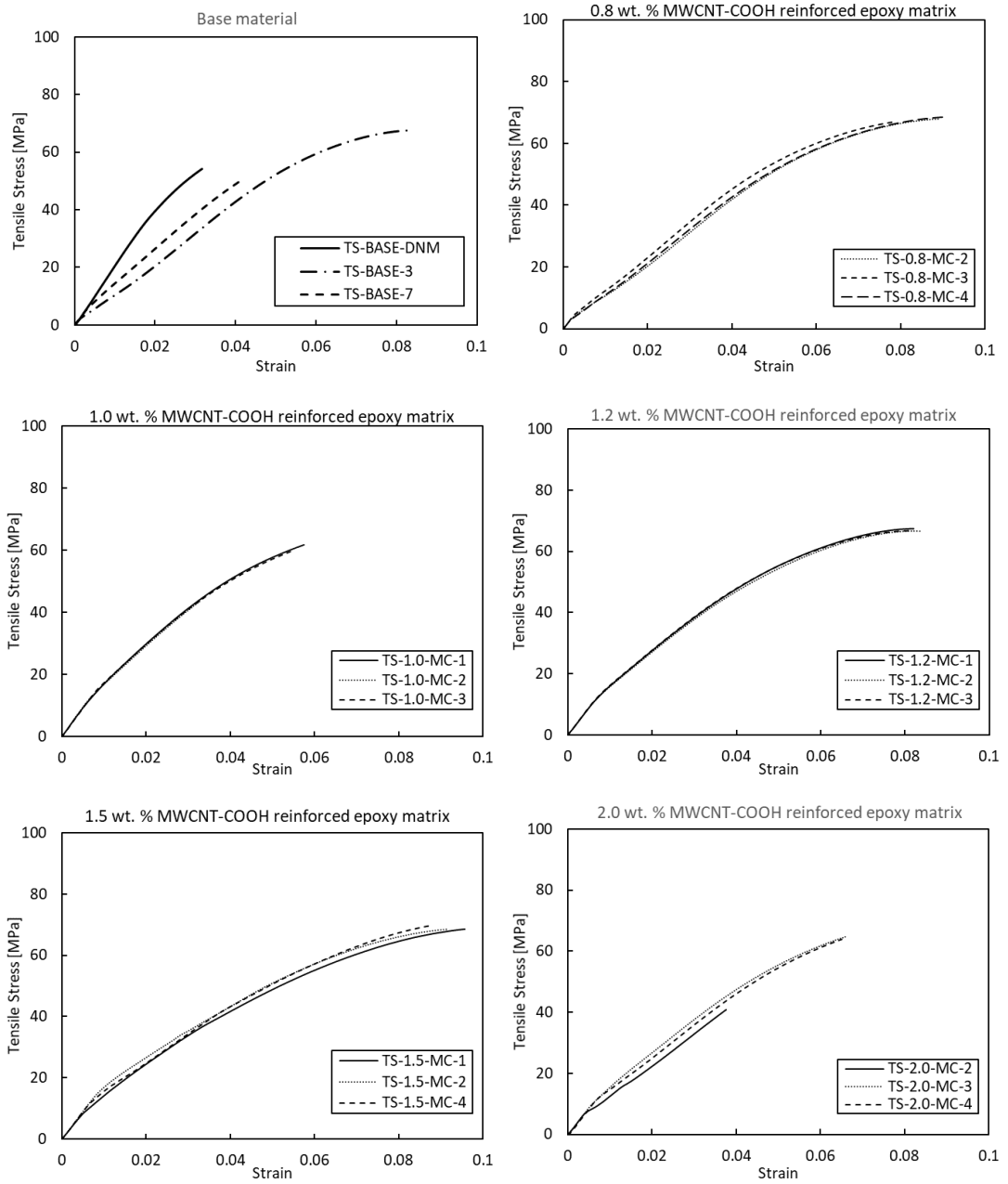


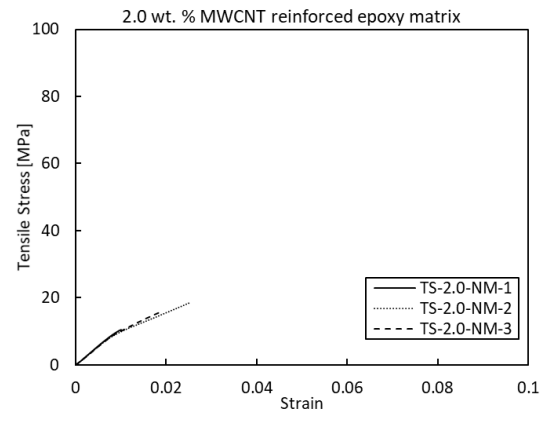
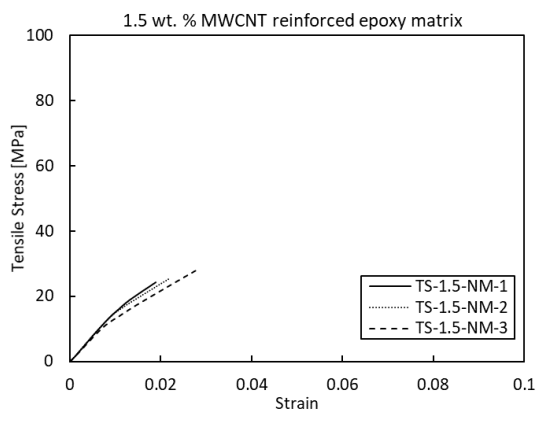
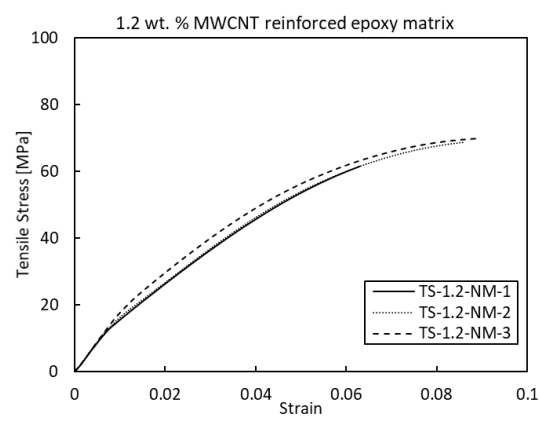
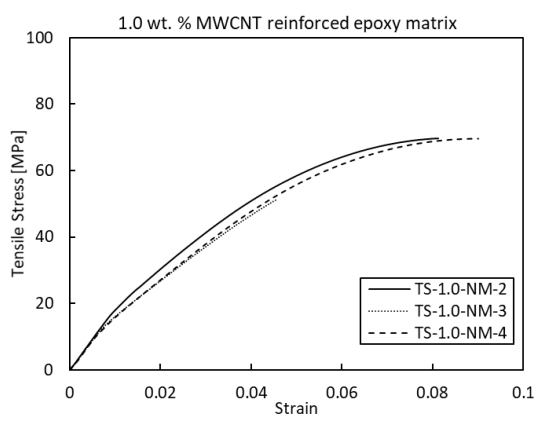
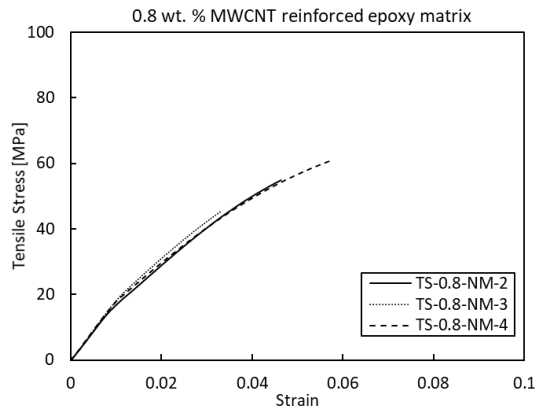
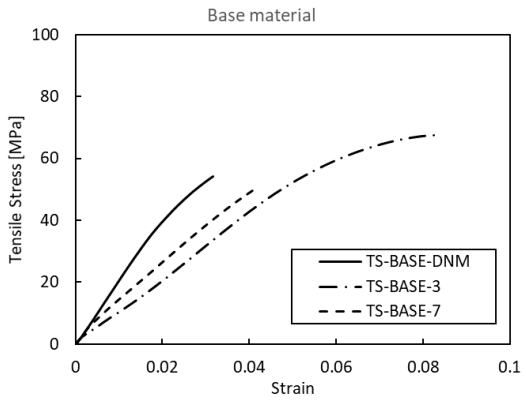
E2. Stress-Strain Plots for Flexural Tests





E3. Stress-Strain Plots for Tensile Tests





E4. Plots for Dynamic Mechanical Analysis

